

# Meson Exchange Currents in $(e, e'p)$ recoil polarization observables

F. Kazemi Tabatabaei<sup>1</sup>, J.E. Amaro<sup>1</sup> and J.A. Caballero<sup>2</sup>

<sup>1</sup> *Departamento de Física Moderna, Universidad de Granada, Granada 18071, Spain*

<sup>2</sup> *Departamento de Física Atómica, Molecular y Nuclear  
Universidad de Sevilla, Apdo. 1065, Sevilla 41080, Spain*

---

## Abstract

A study of the effects of meson-exchange currents and isobar configurations in  $A(\vec{e}, e'\vec{p})B$  reactions is presented. We use a distorted wave impulse approximation (DWIA) model where final-state interactions are treated through a phenomenological optical potential. The model includes relativistic corrections in the kinematics and in the electromagnetic one- and two-body currents. The full set of polarized response functions is analyzed, as well as the transferred polarization asymmetry. Results are presented for proton knock-out from closed-shell nuclei, for moderate to high momentum transfer.

---

*PACS:* 25.30.Fj; 24.10.Eq; 24.70.+s 24.10.Jv

*Keywords:* electromagnetic nucleon knockout; polarized beam; nucleon recoil polarization; final state interactions; meson exchange currents; structure response functions.

# 1 Introduction

For the last decades coincidence  $(e,e'p)$  reactions on complex nuclei have provided precise information on bound nucleon properties, which have made it possible to test carefully the validity of present nuclear models [1, 2, 3, 4]. Although the analysis of these processes, making use of different distorted wave approaches and coupled-channel models, has been extremely useful, there are still uncertainties associated to the various ingredients that enter in the description of the reaction mechanism: treatment of final-state interactions (FSI), nuclear correlations, off-shell effects, Coulomb distortion of the electrons, relativistic degrees of freedom, meson-exchange currents (MEC), etc. All of these ingredients affect the evaluation of the differential cross section and hence lead to ambiguities in the extraction of the spectroscopic factors. The origin of this uncertainty is directly connected with the complexity of the dynamics of the reaction and the different approaches to handle it, which produce different cross sections. It is clear that a reliable determination of spectroscopic factors requires an accurate description of the reaction mechanism. Important efforts in this direction have been done in recent works [5, 6, 7, 8, 9].

The measurement of the separate nuclear response functions and asymmetries imposes additional restrictions over the theory. The exclusive response functions, which include different components of the hadronic tensor taken along the longitudinal (L) or transverse (T) directions with respect to the momentum transfer  $\mathbf{q}$ , may present very different sensitivities to the different aspects of the reaction. In this sense, it is interesting to point out that MEC are shown to contribute mainly to the transverse components [10, 11, 12], while relativistic degrees of freedom play a crucial role in the interference TL response [8, 13]. Thus, a joint analysis of cross sections and response functions, comparing the experimental data with the theoretical predictions, can provide very relevant and complementary information on the reaction mechanism. Separate response functions and the TL asymmetry have been measured for  $^{16}\text{O}(e,e'p)$  at moderate [14, 15] and high [16]  $q$ -values. The asymmetry  $A_{TL}$ , obtained from the difference of cross sections measured at opposite azimuthal angles (with respect to  $\mathbf{q}$ ) divided by the sum, results particularly relevant because it does not depend on the spectroscopic factors. For high missing momentum  $p \geq 300$  MeV/c,  $A_{TL}$  presents an oscillatory structure that has been shown to be consistent with predictions of ‘dynamical’ relativistic calculations [13, 17, 18, 19].

The advent of longitudinally polarized beams [20] and recoil polarization measurements [21, 22] has importantly enlarged the number of observables which can be accessible with this type of experiments, a fact that is welcome to challenge the theory strongly. In recent experiments carried out at MIT-Bates and Jefferson Lab, the induced ( $\mathbf{P}$ ) and transferred ( $\mathbf{P}'$ ) polarization asymmetries were measured for complex nuclei,  $^{12}\text{C}$  [21] and  $^{16}\text{O}$  [22], respectively. In both cases  $(q, \omega)$ -constant kinematics has been selected with  $q \approx 760$  MeV/c,  $\omega \approx 290$  MeV at MIT-Bates and  $q \approx 1000$  MeV/c,  $\omega \approx 450$  MeV at TJlab. Since the transfer momentum values are high enough, relativistic degrees of freedom should be incorporated in a consistent description of these reactions. After the pioneering work in [23, 24], a detailed study on the induced normal polarization  $P_n$  has

been presented in [25, 26] within the framework of the relativistic distorted wave impulse approximation (RDWIA). A comparison with non-relativistic analyses was also discussed. The sensitivity of polarized observables to channel coupling in final state interactions was analyzed in [3, 27], while in [17] the study was focussed on the effects of spinor distortion over the transfer polarization ratio  $P'_x/P'_z$ . In [28] the whole eighteen recoil nucleon polarized responses were computed from intermediate to high momentum transfer in the Dirac eikonal formalism. A comparison between the predictions of the Glauber and eikonal models for  $P_n$  was presented in [29] with the aim of bridge the gap between the low- and high-energy description of FSI. More recently a theoretical study of kinematical and dynamical relativistic effects over polarized response functions and polarization asymmetries has been performed in [30, 31] within the relativistic plane-wave impulse approximation (RPWIA). A general analysis of all the polarized observables within the RDWIA is at present in progress [32].

Our main aim in this work is to explore in depth the role played by the two-body currents in recoil nucleon polarization observables. Some previous analyses on this subject have been done by the Pavia group [33, 34] and the Gent group [35, 36]. The calculation of MEC in [33, 34] makes use of an effective one-body operator leading to results which, in the unpolarized case, differ significantly from those obtained with other approaches that describe properly the two-body currents [37, 38]. Recently the unpolarized model of [34] has been improved in [39], but differences with other MEC calculations still persist [40]. In [36] the induced and transferred polarization asymmetries  $P_n$ ,  $P'_l$  and  $P'_t$  were evaluated for different kinematical situations. The model considered did not rely on any empirical input with respect to the FSI, describing the bound and scattering states as the solutions of the Schrödinger equation with a mean field potential obtained from a Hartree-Fock calculation. MEC were included based on the formalism developed in [37] which also differs from the MEC analysis performed in [38, 40]. In addition, in [36] results for high momentum transfer (up to  $q = 1$  GeV/c) were evaluated including relativistic corrections into the one-body current operator obtained through the Foldy-Wouthuysen method.

In this work we extend the DWIA+MEC model developed for unpolarized reactions in Refs. [38, 40] in order to describe the spin observables in  $(\vec{e}, e'\vec{p})$  processes from closed shell nuclei. This model takes care of relativistic degrees of freedom by making use of semi-relativistic (SR) operators for the one-body (OB) current [13, 41, 42, 43] as well as for the two-body MEC [40, 44, 45, 46]. The SR currents are obtained by a direct Pauli reduction of the corresponding relativistic operators by expanding only in missing momentum over the nucleon mass while treating the transferred energy and momentum exactly. Relativistic kinematics for the ejected nucleon is assumed throughout this work. Finally FSI are incorporated through a phenomenological optical potential which, for high momentum transfer, is taken as the Schrödinger-equivalent form of a S-V Dirac optical potential. The goal of this work is to use the SR approach to evaluate the importance of MEC effects upon the spin observables and their dependence on the FSI for intermediate to high momentum transfer. As a complete relativistic distorted wave analysis of MEC in  $(e, e'p)$  processes is still lacking—the only study in this direction has been performed

taking into account only the contact current [47]— the use of the SR model becomes, as a starting point, a convenient way of implementing relativistic effects in existing non relativistic descriptions of the reaction mechanism in order to explore the high momentum region.

The paper is organized as follows: in Section 2 we outline the DWIA formalism describing in detail the multipole expansion done for the separate response functions. In Section 3 we present our results for the polarized response functions and transferred polarization asymmetries for selected kinematics near the quasielastic peak. Finally our conclusions are drawn in Section 4.

## 2 DWIA model of $(\vec{e}, e'\vec{p})$

### 2.1 Cross section and response functions

The general formalism for coincidence electron scattering on nuclei involving polarization degrees of freedom has been presented in detail in Refs. [4, 23, 24, 48]. In this section we simply provide the basic description of our DWIA model focusing on the development of the multipole expansion used to compute the response functions. For this end we follow closely the multipole formalism developed in [49] for polarized nuclei.

We consider the process depicted in Fig. 1, in which an incident electron with four-momentum  $K_e^\mu = (\epsilon_e, \mathbf{k}_e)$  and helicity  $h$  interacts with a nucleus  $A$ , scatters through an angle  $\theta_e$  to four-momentum  $K_e'^\mu = (\epsilon', \mathbf{k}'_e)$  and is detected in coincidence with a nucleon with momentum  $\mathbf{p}'$  and energy  $E'$ . The four-momentum transferred to the nucleus is  $Q^\mu = K_e^\mu - K_e'^\mu = (\omega, \mathbf{q})$ , verifying  $Q^2 = \omega^2 - q^2 < 0$ . The polarization of the final nucleon is measured along an arbitrary direction defined by the unitary vector  $\mathbf{s}$ . Assuming plane waves for the electrons and neglecting the nuclear recoil, the cross section can be written in the extreme relativistic limit (ERL)  $m_e \ll \epsilon_e$ , as [48]

$$\frac{d\sigma}{d\epsilon'_e d\Omega'_e d\hat{\mathbf{p}}'} = \Sigma + h\Delta, \quad (1)$$

where a separation has been made into terms involving polarized and unpolarized incident electrons. Using the general properties of the leptonic tensor it can be shown that both terms,  $\Sigma$  and  $\Delta$ , have the following decompositions:

$$\Sigma = K\sigma_M \left( v_L R^L + v_T R^T + v_{TL} R^{TL} + v_{TT} R^{TT} \right), \quad (2)$$

$$\Delta = K\sigma_M \left( v_{TL'} R^{TL'} + v_{T'} R^{T'} \right), \quad (3)$$

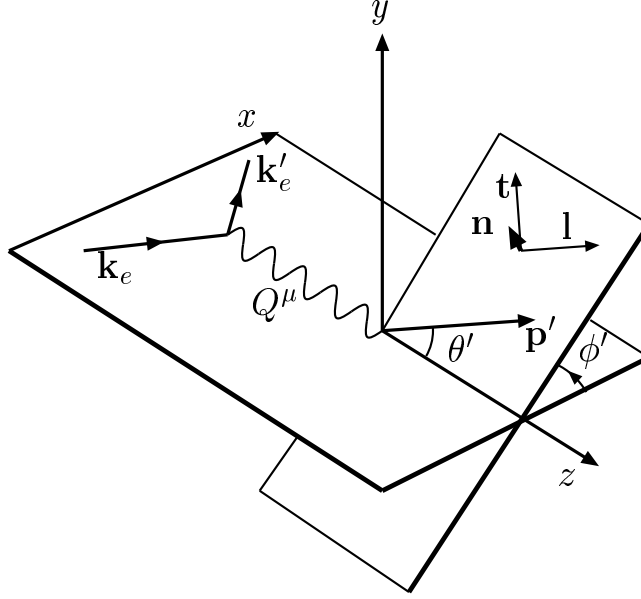


Figure 1: Kinematics for the  $(e, e'p)$  reaction. The  $(x, y, z)$  coordinate system is referred to the scattering plane with the  $z$ -axis lying along the direction of the momentum transfer  $\mathbf{q}$ . The barycentric system  $(l, t, n)$  is referred to the reaction plane:  $\mathbf{l}$  lies along the direction of the ejected nucleon  $\mathbf{p}'$ , the direction  $\mathbf{n}$  is defined by  $\mathbf{q} \times \mathbf{p}'$ , and  $\mathbf{t} = \mathbf{n} \times \mathbf{l}$ .

$\sigma_M$  is the Mott cross section, the factor  $K \equiv m_N p' / (2\pi\hbar)^3$ , with  $m_N$  the nucleon mass, and the  $v_\alpha$ -coefficients are the usual electron kinematical factors<sup>1</sup>.

The hadronic dynamics of the process is contained in the exclusive response functions  $R^K$ , which are given as

$$R^L = W^{00}, \quad R^T = W^{xx} + W^{yy}, \quad (4)$$

$$R^{TL} = \sqrt{2}(W^{0x} + W^{x0}), \quad R^{TT} = W^{yy} - W^{xx}, \quad (5)$$

$$R^{T'} = i(W^{xy} - W^{yx}), \quad R^{TL'} = i\sqrt{2}(W^{0y} + W^{y0}), \quad (6)$$

with  $W^{\mu\nu}$  the hadronic tensor

$$W^{\mu\nu} = \frac{1}{K} \sum_{M_B} \langle \mathbf{p}' \mathbf{s}, B | \hat{J}^\mu(\mathbf{q}) | A \rangle^* \langle \mathbf{p}' \mathbf{s}, B | \hat{J}^\nu(\mathbf{q}) | A \rangle \quad (7)$$

constructed from the matrix elements of the electromagnetic nuclear current operator  $\hat{J}^\mu(\mathbf{q})$  between the ground state of the target nucleus  $|A\rangle$  (assumed to have zero total

<sup>1</sup>In this work we consider the kinematical factors similar to those expressions presented in [48]. Notice that these factors differ from the ones of ref. [24] in a global sign for  $v_{TL}$ ,  $v_{TL'}$  and  $v_{TT}$ , and an additional  $1/\sqrt{2}$  factor in the case of the interference  $TL$  coefficients

angular momentum), and the final hadronic states  $|\mathbf{p}'\mathbf{s}, B\rangle$ . In what follows we assume the residual nucleus to be left in a bound state, hence its wave function can be written down in the form  $|B\rangle = |J_B M_B\rangle$  with  $J_B$  the total angular momentum. The state  $|\mathbf{p}'\mathbf{s}\rangle$  represents the asymptotic distorted wave function of the ejected nucleon polarized along an arbitrary  $\mathbf{s}$ -direction, determined by the angles  $(\theta_s, \phi_s)$  referred to the  $xyz$  coordinate system of Fig. 1. It is given by

$$|\mathbf{p}'\mathbf{s}\rangle = \sum_{\nu=-1/2}^{1/2} \mathcal{D}_{\nu\frac{1}{2}}^{(1/2)}(\theta_s, \phi_s, 0) |\mathbf{p}'\nu\rangle, \quad (8)$$

where  $|\mathbf{p}'\nu\rangle$  is referred to the system with the quantization axis along  $\mathbf{q}$  and the arguments of the rotation matrices are the Euler angles that specify the  $\mathbf{s}$ -direction.

Isolating the explicit dependences on the azimuthal angle of the ejected nucleon  $\phi' = \phi$ , the hadronic responses can be expressed in the form

$$R^L = W^L \quad (9)$$

$$R^T = W^T \quad (10)$$

$$R^{TL} = \cos\phi W^{TL} + \sin\phi \widetilde{W}^{TL} \quad (11)$$

$$R^{TT} = \cos 2\phi W^{TT} + \sin 2\phi \widetilde{W}^{TT} \quad (12)$$

$$R^{T'} = \widetilde{W}^{T'} \quad (13)$$

$$R^{TL'} = \cos\phi \widetilde{W}^{TL'} + \sin\phi W^{TL'}, \quad (14)$$

where the functions  $W^K$  and  $\widetilde{W}^K$  are totally specified by four kinematical variables, for instance  $\{E, \omega, q, \theta'\}$ , and the polarization direction  $\{\theta_s, \Delta\phi = \phi - \phi_s\}$ . The responses with and without tilde refer to their dependence on the spin vector  $\mathbf{s}$ . As shown below,  $\widetilde{W}^K$  are purely spin-vector, while  $W^K$  present also a spin-scalar dependence, so only the latter survive when the polarization of the ejected nucleon is not measured.

In the case of  $(\vec{e}, e'\vec{N})$  processes, the hadronic response functions are usually given by referring the recoil nucleon polarization vector  $\mathbf{s}$  to the baryocentric system defined by the axes (see Fig. 1):  $\mathbf{l}$  (along the  $\mathbf{p}'$  direction),  $\mathbf{n}$  (normal direction to the plane defined by  $\mathbf{q}$  and  $\mathbf{p}'$ , i.e., along  $\mathbf{q} \times \mathbf{p}'$ ) and  $\mathbf{t}$  (determined by  $\mathbf{n} \times \mathbf{l}$ )<sup>2</sup>. It can be shown (see Refs. [23, 24] for details) that a total of eighteen response functions enter in the analysis of  $(\vec{e}, e'\vec{N})$  reactions. These are given by the decomposition

$$W^K = \frac{1}{2} W_{unpol}^K + W_n^K s_n, \quad K = L, T, TL, TT, TL', \quad (15)$$

$$\widetilde{W}^K = W_l^K s_l + W_t^K s_t, \quad K = TL, TT, T', TL', \quad (16)$$

---

<sup>2</sup>Notice that this notation does not coincide with Refs. [30, 31] where the  $\mathbf{t}$  direction is denoted as  $\mathbf{s}$  (sideways)

where, as mentioned above, only the  $W_{unpol}^K$  responses survive within the unpolarized case. Moreover,  $W_{unpol}^{TL'}$  (referred as fifth response) enters only when the polarization of the incident electron is measured.

Owing to the above decomposition, the response functions (9–14) can be expressed in the form  $R^K = R_{unpol}^K/2 + \mathbf{R}^K \cdot \mathbf{s}$ , and similarly, the cross section (1–3) can be written as a sum of unpolarized and spin-vector dependent terms

$$\frac{d\sigma}{d\epsilon'_e d\Omega'_e d\hat{\mathbf{p}}'} = \frac{1}{2}\Sigma_{unpol} + \boldsymbol{\Sigma} \cdot \mathbf{s} + h \left( \frac{1}{2}\Delta_{unpol} + \boldsymbol{\Delta} \cdot \mathbf{s} \right) \quad (17)$$

$$= \frac{1}{2}\Sigma_{unpol} [1 + \mathbf{P} \cdot \mathbf{s} + h(A + \mathbf{P}' \cdot \mathbf{s})] , \quad (18)$$

where the usual polarization asymmetries have been introduced [3]:

$$\mathbf{P} = \boldsymbol{\Sigma} / \left( \frac{1}{2}\Sigma_{unpol} \right) \quad \text{Induced polarization,} \quad (19)$$

$$\mathbf{P}' = \boldsymbol{\Delta} / \left( \frac{1}{2}\Sigma_{unpol} \right) \quad \text{Transferred polarization,} \quad (20)$$

$$A = \Delta_{unpol} / \Sigma_{unpol} \quad \text{Electron analyzing power.} \quad (21)$$

## 2.2 Multipole analysis of response functions

In this section we present the multipole expansion of the response functions to be used in our DWIA model. The final expressions, where the sums over third components of angular momenta have been performed analytically, result convenient in the present work since the computational time can be considerably reduced, specially the calculation concerning the MEC. Note that the number of multipoles needed to get convergence increases with  $q, \omega$  and up to  $\sim 36$  multipoles are needed for  $q = 1$  GeV/c. The expansion is performed following the formalism developed in [49] for exclusive reactions from polarized nuclei. A basic difference between the present work and that of ref. [49] lies on the sums performed over the third components which are different when initial and/or final state polarizations are considered. Here we simply present the final expressions, referring to ref. [49] for details on the expansion method and to the Appendix for an outline on the procedure used to perform the sum over third components in the present case.

In order to compute the hadronic tensor in our DWIA model we first perform a multipole expansion of the ejected nucleon wave function in partial waves. The final hadronic states may then be written

$$|\mathbf{p}'\nu, B\rangle = \sum_{lMj m_p J_f M_f} i^l Y_{lM}^*(\hat{\mathbf{p}}') \langle \frac{1}{2}\nu l M | j m_p \rangle \langle j m_p J_B M_B | J_f M_f \rangle |(l j) J_B, J_f M_f\rangle , \quad (22)$$

where the partial waves ( $lj$ ) are coupled to the angular momentum  $J_B$  of the residual nucleus to give a total angular momentum  $J_f$  in the final states  $|f\rangle = |(lj)J_B, J_f M_f\rangle$ .

The electromagnetic charge and transverse current operators are expanded as sums involving Coulomb (C), electric (E) and magnetic (M) tensor operators,

$$\hat{\rho}(q) = \sqrt{4\pi} \sum_{J=0}^{\infty} i^J [J] \hat{M}_{J0}(q) \quad (23)$$

$$\hat{J}_m = -\sqrt{2\pi} \sum_{J=1}^{\infty} i^J [J] \left[ \hat{T}_{Jm}^{el}(q) + m \hat{T}_{Jm}^{mag}(q) \right], \quad m = \pm 1, \quad (24)$$

where, as usual, we assume the transfer momentum  $\mathbf{q}$  along the  $z$ -direction and  $\hat{J}_m$  are the spherical components of the current operator  $\hat{\mathbf{J}}$ . We use the bracket symbol  $[J] = \sqrt{2J+1}$  for angular momenta. Inserting (8,22,23,24) into the hadronic tensor (7), the following expansion for the responses  $W^K$  and  $\widetilde{W}^K$  is obtained

$$W^K = \frac{1}{2} W_{unpol}^K + 2\pi P_1^1(\cos\theta_s) \sin(\Delta\phi) \widetilde{W}_{11}^K, \quad (25)$$

for  $K = L, T, TL, TT, TL'$ , and

$$\widetilde{W}^K = 2\pi\alpha_K \left[ P_1^0(\cos\theta_s) W_{10}^K + P_1^1(\cos\theta_s) \cos(\Delta\phi) W_{11}^K \right] \quad (26)$$

for  $K = TL, TT, T', TL'$ , with the coefficient  $\alpha_K = -1$  for  $TL, TT$  and  $\alpha_K = 1$  for  $T', TL'$ , and  $P_J^M(\cos\theta_s)$  the Legendre functions.

The five response functions  $W_{unpol}^K$  are the only ones that survive when summing over final spins  $\pm s$ , in which case the  $1/2$  factor cancels and the unpolarized cross section is recovered. The spin dependence is determined from the thirteen reduced response functions  $W_{1\mathcal{M}}^K$  ( $\mathcal{M} = 0, 1$ ) and  $\widetilde{W}_{11}^K$  introduced above. Explicit expressions for these reduced responses can be written in terms of the reduced matrix elements of the current multipole operators

$$C_\sigma = \langle (lj)J_B, J | \hat{M}_J | 0 \rangle \quad (27)$$

$$E_\sigma = \langle (lj)J_B, J | \hat{T}_J^{el} | 0 \rangle \quad (28)$$

$$M_\sigma = \langle (lj)J_B, J | i \hat{T}_J^{mag} | 0 \rangle, \quad (29)$$

where we have defined a multiple index  $\sigma = (l, j, J)$  corresponding to the quantum numbers of the final states. Note that the initial state  $|A\rangle = |0\rangle$  has total angular momentum equal to zero, so  $J_f = J$ . The response functions involve quadratic products of these



multipole matrix elements which can be decomposed into their real ( $R_{\sigma'\sigma}^K$ ) and imaginary ( $I_{\sigma'\sigma}^K$ ) parts:

$$C_{\sigma'}^* C_{\sigma} = R_{\sigma'\sigma}^L + iI_{\sigma'\sigma}^L \quad (30)$$

$$E_{\sigma'}^* E_{\sigma} + M_{\sigma'}^* M_{\sigma} = R_{\sigma'\sigma}^{T1} + iI_{\sigma'\sigma}^{T1} \quad (31)$$

$$E_{\sigma'}^* M_{\sigma} - M_{\sigma'}^* E_{\sigma} = R_{\sigma'\sigma}^{T2} + iI_{\sigma'\sigma}^{T2} \quad (32)$$

$$C_{\sigma'}^* E_{\sigma} = R_{\sigma'\sigma}^{TL1} + iI_{\sigma'\sigma}^{TL1} \quad (33)$$

$$C_{\sigma'}^* M_{\sigma} = R_{\sigma'\sigma}^{TL2} + iI_{\sigma'\sigma}^{TL2} \quad (34)$$

$$E_{\sigma'}^* E_{\sigma} - M_{\sigma'}^* M_{\sigma} = R_{\sigma'\sigma}^{TT1} + iI_{\sigma'\sigma}^{TT1} \quad (35)$$

$$E_{\sigma'}^* M_{\sigma} + M_{\sigma'}^* E_{\sigma} = R_{\sigma'\sigma}^{TT2} + iI_{\sigma'\sigma}^{TT2}. \quad (36)$$

Expressions for the unpolarized response functions  $W_{unpol}^K$  in terms of (30–36) are given in ref. [41], while the recoil nucleon polarized responses can be written as

$$\widetilde{W}_{11}^L = \frac{1}{K} \sum_{J'L} \tilde{h}_{1J'L0}^1(\theta') \sum_{\sigma'\sigma} P_{l+l'+J'}^+ \Phi_{\sigma'\sigma} \begin{pmatrix} J' & J & L \\ 0 & 0 & 0 \end{pmatrix} \xi_{J'-l',J-l}^+ I_{\sigma'\sigma}^L \quad (37)$$

$$\begin{aligned} \widetilde{W}_{11}^T &= -\frac{1}{K} \sum_{J'L} P_{J'+L}^+ \tilde{h}_{1J'L0}^1(\theta') \sum_{\sigma'\sigma} P_{l+l'+J'}^+ \Phi_{\sigma'\sigma} \begin{pmatrix} J' & J & L \\ 1 & -1 & 0 \end{pmatrix} \\ &\times \left( \xi_{J'-l',J-l}^+ I_{\sigma'\sigma}^{T1} + \xi_{J'-l',J-l}^- I_{\sigma'\sigma}^{T2} \right) \end{aligned} \quad (38)$$

$$\begin{aligned} \widetilde{W}_{11}^{TL} &= -\frac{1}{K} 2\sqrt{2} \sum_{J'L} (-1)^{J'+L} \tilde{h}_{1J'L1}^1(\theta') \sum_{\sigma'\sigma} P_{l+l'+J'}^+ \Phi_{\sigma'\sigma} \begin{pmatrix} J' & J & L \\ 0 & 1 & -1 \end{pmatrix} \\ &\times \left( \xi_{J'-l',J-l}^+ I_{\sigma'\sigma}^{TL1} - \xi_{J'-l',J-l}^- I_{\sigma'\sigma}^{TL2} \right) \end{aligned} \quad (39)$$

$$\begin{aligned} \widetilde{W}_{11}^{TT} &= -\frac{1}{K} \sum_{J'L} (-1)^{J'+L} \tilde{h}_{1J'L2}^1(\theta') \sum_{\sigma'\sigma} P_{l+l'+J'}^+ \Phi_{\sigma'\sigma} \begin{pmatrix} J' & J & L \\ 1 & 1 & -2 \end{pmatrix} \\ &\times \left( \xi_{J'-l',J-l}^+ I_{\sigma'\sigma}^{TT1} - \xi_{J'-l',J-l}^- I_{\sigma'\sigma}^{TT2} \right) \end{aligned} \quad (40)$$

$$\begin{aligned} \widetilde{W}_{11}^{TL'} &= -\frac{1}{K} 2\sqrt{2} \sum_{J'L} (-1)^{J'+L} \tilde{h}_{1J'L1}^1(\theta') \sum_{\sigma'\sigma} P_{l+l'+J'}^+ \Phi_{\sigma'\sigma} \begin{pmatrix} J' & J & L \\ 0 & 1 & -1 \end{pmatrix} \\ &\times \left( \xi_{J'-l',J-l}^+ R_{\sigma'\sigma}^{TL1} - \xi_{J'-l',J-l}^- R_{\sigma'\sigma}^{TL2} \right) \end{aligned} \quad (41)$$

$$\begin{aligned} W_{1M}^{TL} &= -\frac{1}{K} 2\sqrt{2} \sum_{J'L} (-1)^{J'+L} h_{1J'L1}^M(\theta') \sum_{\sigma'\sigma} P_{l+l'+J'}^+ \Phi_{\sigma'\sigma} \begin{pmatrix} J' & J & L \\ 0 & 1 & -1 \end{pmatrix} \\ &\times \left( \xi_{J'-l',J-l}^+ I_{\sigma'\sigma}^{TL1} - \xi_{J'-l',J-l}^- I_{\sigma'\sigma}^{TL2} \right) \end{aligned} \quad (42)$$

$$\begin{aligned} W_{1M}^{TT} &= -\frac{1}{K} \sum_{J'L} (-1)^{J'+L} h_{1J'L2}^M(\theta') \sum_{\sigma'\sigma} P_{l+l'+J'}^+ \Phi_{\sigma'\sigma} \begin{pmatrix} J' & J & L \\ 1 & 1 & -2 \end{pmatrix} \\ &\times \left( \xi_{J'-l',J-l}^+ I_{\sigma'\sigma}^{TT1} - \xi_{J'-l',J-l}^- I_{\sigma'\sigma}^{TT2} \right) \end{aligned} \quad (43)$$

$$\begin{aligned}
W_{1\mathcal{M}}^{T'} &= -\frac{1}{K} \sum_{\mathcal{J}'L} P_{\mathcal{J}'L}^- h_{1\mathcal{J}'L0}^{\mathcal{M}}(\theta') \sum_{\sigma'\sigma} P_{l+l'+\mathcal{J}'}^+ \Phi_{\sigma'\sigma} \begin{pmatrix} J' & J & L \\ 1 & -1 & 0 \end{pmatrix} \\
&\quad \times \left( \xi_{J'-l',J-l}^+ R_{\sigma'\sigma}^{T1} + \xi_{J'-l',J-l}^- R_{\sigma'\sigma}^{T2} \right) \tag{44}
\end{aligned}$$

$$\begin{aligned}
W_{1\mathcal{M}}^{TL'} &= -\frac{1}{K} 2\sqrt{2} \sum_{\mathcal{J}'L} (-1)^{\mathcal{J}'+L} h_{1\mathcal{J}'L1}^{\mathcal{M}}(\theta') \sum_{\sigma'\sigma} P_{l+l'+\mathcal{J}'}^+ \Phi_{\sigma'\sigma} \begin{pmatrix} J' & J & L \\ 0 & 1 & -1 \end{pmatrix} \\
&\quad \times \left( \xi_{J'-l',J-l}^+ R_{\sigma'\sigma}^{TL1} - \xi_{J'-l',J-l}^- R_{\sigma'\sigma}^{TL2} \right), \tag{45}
\end{aligned}$$

where we use the parity functions

$$P_n^\pm = (1 \pm (-1)^n)/2, \quad \xi_{J'J}^+ \equiv (-1)^{(J'-J)/2} P_{J'+J}^+, \quad \xi_{J'J}^- \equiv (-1)^{(J'-J+1)/2} P_{J'+J}^- \tag{46}$$

and the angular dependence of the above responses is determined by the functions  $h_{\mathcal{J}\mathcal{J}'LM}^{\mathcal{M}}(\theta')$  and  $\tilde{h}_{\mathcal{J}\mathcal{J}'LM}^{\mathcal{M}}(\theta')$ , defined through the coupling of two spherical harmonics (see (88)).

$$\begin{aligned}
\text{Re}[Y_{\mathcal{J}}(\mathbf{s})Y_{\mathcal{J}'}(\hat{\mathbf{p}}')]_{LM} &= \cos M\phi' \sum_{\mathcal{M}=0}^{\mathcal{J}} h_{\mathcal{J}\mathcal{J}'LM}^{\mathcal{M}}(\theta') P_{\mathcal{J}}^{\mathcal{M}}(\cos\theta_s) \cos(\mathcal{M}\Delta\phi) \\
&\quad + \sin M\phi' \sum_{\mathcal{M}=0}^{\mathcal{J}} \tilde{h}_{\mathcal{J}\mathcal{J}'LM}^{\mathcal{M}}(\theta') P_{\mathcal{J}}^{\mathcal{M}}(\cos\theta_s) \sin(\mathcal{M}\Delta\phi). \tag{47}
\end{aligned}$$

Finally, the coefficients  $\Phi_{\sigma'\sigma}$  are derived in the Appendix and are given by eq. (86) selecting  $\mathcal{J} = 1$ . Although the above expressions correspond formally to those denoted as  $W_{\mathcal{J}\mathcal{M}}^{K(-)}$  and  $\tilde{W}_{\mathcal{J}\mathcal{M}}^{K(-)}$  in [49] for polarized nuclei and  $\mathcal{J} = 1$ , it is important to point out that the coefficients  $\Phi_{\sigma'\sigma}$  contain the whole information on the polarization distribution of the particles. Hence the significance of  $\Phi_{\sigma'\sigma}$  is clearly different when polarization degrees of freedom are considered for the ejected nucleon (present work) or the target nucleus [49].

The nuclear structure information in (37-45) is contained in the quadratic forms (30-36) of the  $C$ ,  $E$ ,  $M$  multipoles<sup>3</sup>. Thus the present expansion can be applied to any nuclear model of the reaction as far as it provides multipole matrix elements (27,28,29) for high enough angular momenta  $\sigma = (l, j, J)$ . Note that only the responses involving the real parts  $R_{\sigma'\sigma}^K$  survive when FSI are neglected since in this case all the  $C$ ,  $E$ ,  $M$  multipoles are strictly real functions. Therefore those responses which depend on the imaginary parts are expected to be particularly sensitive to the description of FSI.

Writing down explicitly the Legendre polynomials involved in the multipole expansion (25,26), and comparing with the general expression (15,16), we get the following relation between both sets of response functions:

$$W_n^K = -2\pi \tilde{W}_{11}^K, \quad K = L, T, TL, TT, TL' \tag{48}$$

$$W_l^K = 2\pi\alpha_K \left( W_{11}^K \sin\theta' + W_{10}^K \cos\theta' \right), \quad K = TL, TT, TL', T' \tag{49}$$

$$W_t^K = 2\pi\alpha_K \left( W_{11}^K \cos\theta' - W_{10}^K \sin\theta' \right), \quad K = TL, TT, TL', T' \tag{50}$$

---

<sup>3</sup>Note that there is a typo in eqs. (40-51) of ref. [49]: the order of  $J$  and  $J'$  in the three-j should be reversed. This error has been corrected in eqs. (37-45) in the present paper.

with  $\alpha_K$  as introduced in (26).

### 2.3 Electromagnetic operators and PWIA

In this work we evaluate the exclusive polarized responses using a semi-relativistic (SR) model for describing the electromagnetic one-body (OB) and two-body MEC current operators. The OB current has been obtained by a direct Pauli reduction of the fully relativistic operator in powers only of the initial nucleon momentum over the nucleon mass  $\mathbf{p}/m_N$ . The dependence on the transfer and final momenta, which can be large [42, 43, 44, 45], is treated exactly. The SR-OB current in momentum space can be written as

$$J^0(\mathbf{p}', \mathbf{p}) = \rho_c + i\rho_{so}(\cos\phi\sigma_x - \sin\phi\sigma_y)\chi \quad (51)$$

$$J^x(\mathbf{p}', \mathbf{p}) = iJ_m\sigma_y + J_c\chi\cos\phi \quad (52)$$

$$J^y(\mathbf{p}', \mathbf{p}) = -iJ_m\sigma_x + J_c\chi\sin\phi, \quad (53)$$

where  $\chi = (p/m_N)\sin\theta$ , and  $(\theta, \phi)$  are the angles determining the direction of the initial momentum  $\mathbf{p}$  in the  $(x, y, z)$  coordinate system. The charge ( $\rho_c$ ), spin-orbit ( $\rho_{so}$ ), magnetization ( $J_m$ ) and convection ( $J_c$ ) terms shown above include relativistic corrections and are given by the following expressions

$$\rho_c = \frac{\kappa}{\sqrt{\tau}}G_E, \quad \rho_{so} = \kappa\frac{2G_M - G_E}{2\sqrt{1+\tau}} \quad (54)$$

$$J_m = \sqrt{\tau}G_M, \quad J_c = \frac{\sqrt{\tau}}{\kappa}G_E, \quad (55)$$

where  $\kappa = q/2m_N$ ,  $\tau = |Q^2|/4m_N^2$ , and  $G_E$ ,  $G_M$  are the electric and magnetic nucleon form factors for which we take the Galster parameterization [50].

The two-body MEC operators of pionic (P), seagull or contact (S) and  $\Delta$ -isobar kinds, displayed in the Feynman diagrams of Fig. 2, have been also obtained by making use of a SR approach leading to simple prescriptions that include relativistic corrections through a multiplicative factor (see Refs. [40, 45, 46] for details on the SR expansion method)

$$\mathbf{J}_{SR}^{MEC} = \frac{1}{\sqrt{1+\tau}}\mathbf{J}_{NR}^{MEC}, \quad (56)$$

where  $\mathbf{J}_{NR}^{MEC}$  is the traditional non-relativistic MEC operator.

The expressions for the reduced matrix elements of the OB and MEC multipole operators (27,28,29) in the shell model are given in Refs. [10, 11, 43] except for the relativistic correction factors appearing within the SR operators. The somewhat complex structure displayed by these multipoles makes it not possible to predict the relative importance of

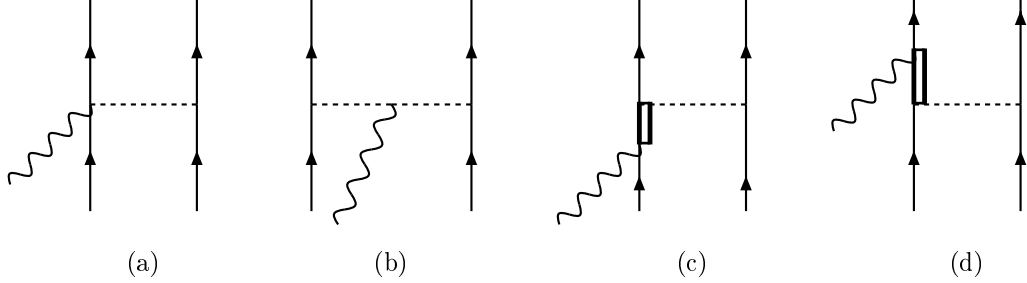


Figure 2: MEC diagrams contributing to the two-body current of this work: seagull (a), pion in flight (b) and  $\Delta$  (c,d) currents are considered including relativistic corrections.

each contribution separately without explicit numerical evaluation, even in the case of the OB current.

Although in this work we perform a DWIA analysis of the response functions, we may take advantage of the significant simplifications introduced within the plane wave impulse approximation (PWIA), where analytical expressions for the response functions can be obtained [30, 31]. First, for intermediate to high values of  $q$ , the PWIA approach is expected to provide reasonable results, thus the analytical PWIA expressions allow us to estimate the contributions of the different pieces of the currents to the polarized response functions. Second, since the PWIA results should be recovered using the present multipole expansion in the limit of no FSI, the comparison between our calculation and the analytical PWIA responses makes it possible to fix the number of multipoles needed to get convergence.

Hence, within PWIA, the matrix element of the OB current is written as

$$\langle \mathbf{p}' \mathbf{s}, B | J^\mu(\mathbf{q}) | A \rangle = \sum_{\beta' \beta} \mathcal{D}_{\beta' \frac{1}{2}}^*(\mathbf{s}) J^\mu(\mathbf{p}', \mathbf{p})_{\beta' \beta} \langle B | a_{\mathbf{p}, \beta} | A \rangle, \quad (57)$$

where  $a_{\mathbf{p}, \beta}$  is the annihilation operator corresponding to a particle with momentum  $\mathbf{p}$  and spin projection  $\beta$  referred to the quantization axis. Inserting this expression into the hadronic tensor (7), and following the procedure described in [43], we obtain

$$W^{\mu\nu} = \frac{1}{2} m_N p' w^{\mu\nu}(\mathbf{p}', \mathbf{p}, \mathbf{s}) M^S(\mathbf{p}), \quad (58)$$

where we have defined the polarized single-nucleon tensor

$$w^{\mu\nu}(\mathbf{p}', \mathbf{p}, \mathbf{s}) = \sum_{\alpha \alpha' \beta'} \mathcal{D}_{\beta' \frac{1}{2}}^*(\mathbf{s}) J^\nu(\mathbf{p}', \mathbf{p})_{\beta' \alpha} J^\mu(\mathbf{p}', \mathbf{p})_{\alpha' \alpha}^* \mathcal{D}_{\alpha' \frac{1}{2}}(\mathbf{s}). \quad (59)$$

In the case of interest here, a closed-shell nucleus, the scalar momentum distribution  $M^S(\mathbf{p})$  for nucleon knock-out from a shell  $nlj$  is given by

$$M^S(\mathbf{p}) = \frac{2j+1}{4\pi} \tilde{R}^2(p) \quad (60)$$

with  $\tilde{R}(p)$  the radial wave function of the hole in momentum space.

Using the current matrix elements (51,52,53) one can compute in the factorized approximation (58) the response functions (4-6). From these results the PWIA expressions for the reduced response functions can be identified. Expressions for the unpolarized responses in PWIA were given in [43, 49]. In the case of the polarized responses, from the total of eighteen, only five survive in PWIA. These are given by

$$W_{11}^{T'} = \frac{m_N p'}{4\pi} 2J_c J_m \chi M^S(\mathbf{p}) \quad (61)$$

$$W_{10}^{T'} = \frac{m_N p'}{4\pi} 2J_m^2 M^S(\mathbf{p}) \quad (62)$$

$$\tilde{W}_{11}^{TL'} = \frac{m_N p'}{4\pi} 2\sqrt{2}(\rho_c J_m - \rho_{so} J_c \chi^2) M^S(\mathbf{p}) \quad (63)$$

$$W_{11}^{TL'} = \frac{m_N p'}{4\pi} 2\sqrt{2} \rho_c J_m M^S(\mathbf{p}) \quad (64)$$

$$W_{10}^{TL'} = \frac{m_N p'}{4\pi} 2\sqrt{2} \rho_{so} J_m \chi M^S(\mathbf{p}), \quad (65)$$

where we have used the factors introduced in (54,55). Notice that all the  $L, T, TL$  and  $TT$ -type polarized responses are zero in this approximation.

### 3 Results

In this section we present results for selected recoil nucleon polarization observables corresponding to proton knockout from the  $p_{1/2}$  and  $p_{3/2}$  shells in  $^{16}\text{O}$ . In particular, we restrict ourselves to the analysis of all the polarized response functions, including the fifth response  $W_0^{TL'}$  that does not depend on the nucleon polarization and only enters when the initial electron beam is polarized, and the transferred polarization asymmetries  $P'_{l,t,n}$ . The study of cross sections and induced polarizations will be presented in a forthcoming publication [51]. Two different kinematical situations corresponding to  $(q, \omega)$ -constant kinematics (also referred as quasiperpendicular kinematics) have been selected: i)  $q = 460$  MeV/c,  $\omega = 100$  MeV, and ii)  $q = 1$  GeV/c,  $\omega = 450$  MeV. In both cases the value of the transfer energy  $\omega$  corresponds almost to the quasielastic peak.

In this work our main interest is focused on the role of the two-body MEC operators upon the recoil nucleon polarization observables, trying to identify kinematical conditions

for which these effects can be important; however, a brief excursion on the FSI effects is also presented. All the calculations have been done within the formalism described in the previous section, i.e., semirelativistic expressions for the one- and two-body current operators and a multipole expansion method have been used. The number of multipoles needed has been fixed by comparing the DWIA results, in the particular case of no FSI, with the exact factorized PWIA responses (61–65). Convergence in the multipole analysis is obtained with  $J_{max} = 30$  for  $q = 460$  MeV/c, and  $J_{max} = 35$  for  $q = 1000$  MeV/c. Finally, in all of the results which follow, the kinematics of the ejected nucleon is treated exactly.

### 3.1 Polarized response functions

Here we analyze the thirteen responses defined in (48–50) which arise from the ejected nucleon polarization, plus the “fifth” response function  $W_o^{TL'}$ . Results are displayed in Figs. 3–12. A similar analysis for the unpolarized responses  $L$ ,  $T$ ,  $TL$  and  $TT$  has been performed recently in [40].

#### 3.1.1 Effects of FSI

We start our discussion with the effects of FSI on the polarized responses. A study of the dependence of the unpolarized responses on the particular FSI model was already presented in [38]. In Fig. 3 we show the eight induced polarized responses for proton knock-out from the  $1p_{1/2}$  shell in  $^{16}\text{O}$  as function of the missing momentum  $p$ . Kinematics corresponds to  $q = 460$  MeV/c and  $\omega = 100$  MeV. The five transferred polarized responses plus the fifth one ( $T'$  and  $TL'$  types) are displayed in Fig. 4. Similar results are obtained for the  $1p_{3/2}$  shell and thus they are not shown here. In all of these results we use bound wave functions obtained as solutions of the Schrödinger equation with a Woods-Saxon potential, with parameters taken from ref. [42]. For the final states we use solutions for two different optical potentials. Solid lines correspond to calculations performed with the Comfort and Karp potential [52], which was originally fitted to elastic proton scattering from  $^{12}\text{C}$  for energies below 183 MeV. We have extended it to  $^{16}\text{O}$  by introducing a dependence  $A^{1/3}$  in the radius parameters. The results shown with dashed lines have been computed with the Schwandt potential [53], which also has been extrapolated here for  $^{16}\text{O}$  since it was originally fitted to higher mass nuclei.

The induced polarized  $L$ ,  $T$ ,  $TL$ ,  $TT$  and the fifth response functions, which are zero in absence of FSI, are expected to be highly sensitive to the details of the particular optical potential considered, and in particular, to the spin-orbit term in the potential. In this sense notice the significant difference introduced by both potentials in the case of the polarized  $TL$  and  $TT$  responses (fig. 3), while the FSI discrepancy gets smaller for the fifth response function (fig. 4) and is considerably reduced for  $W_n^L$  and  $W_n^T$ .

$^{16}\text{O}$ ,  $1p_{1/2}$ ,  $q = 460$  MeV/c,  $\omega = 100$  MeV

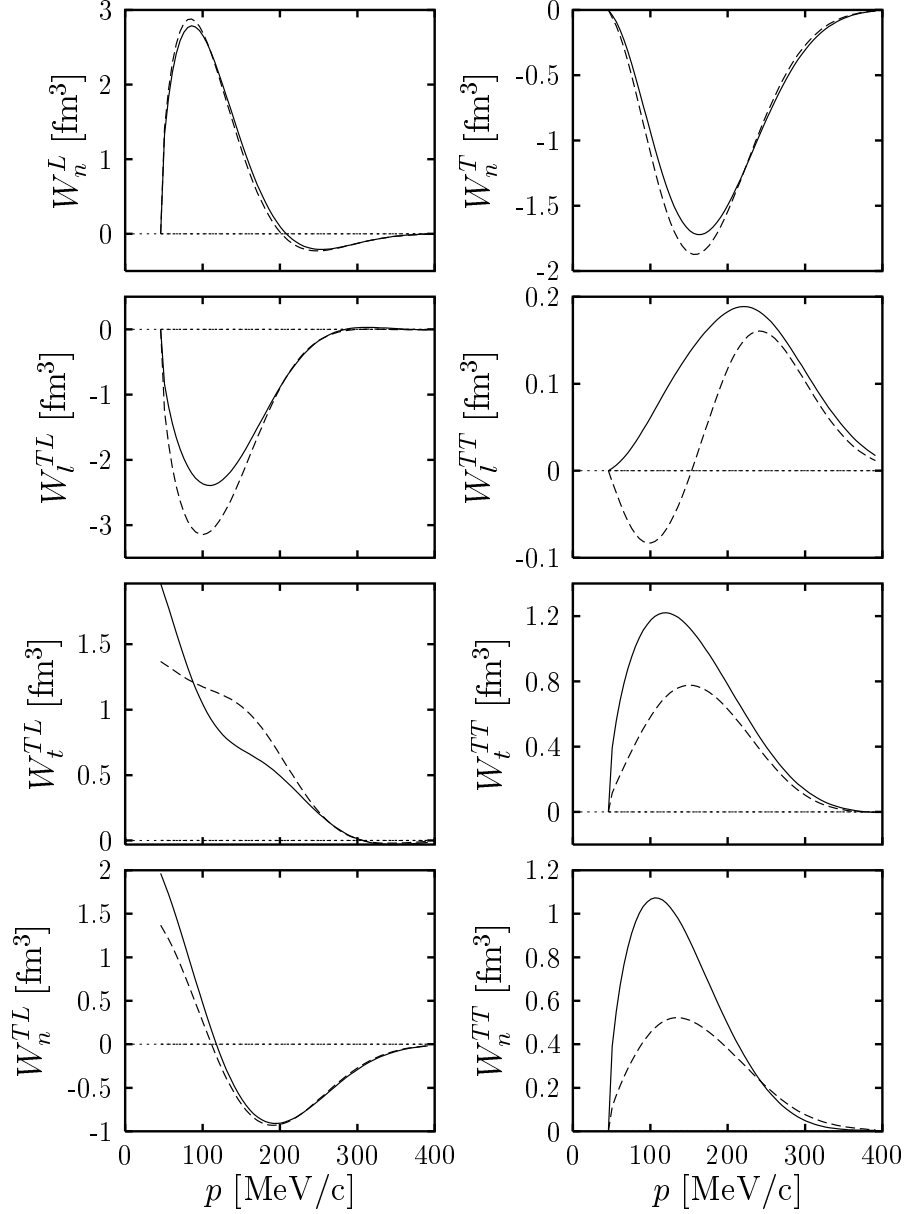


Figure 3: Induced polarized response functions ( $L$ ,  $T$ ,  $TL$  and  $TT$ -type responses) for proton knock-out from the  $1p_{1/2}$  shell in  $^{16}\text{O}$ , with momentum transfer  $q = 460$  MeV/c and energy transfer  $\omega = 100$  MeV. Solid lines are the DWIA results using the optical potential of Comfort and Karp; dashed lines have been computed with the Schwandt optical potential.

$^{16}\text{O}$ ,  $1p_{1/2}$ ,  $q = 460$  MeV/c,  $\omega = 100$  MeV

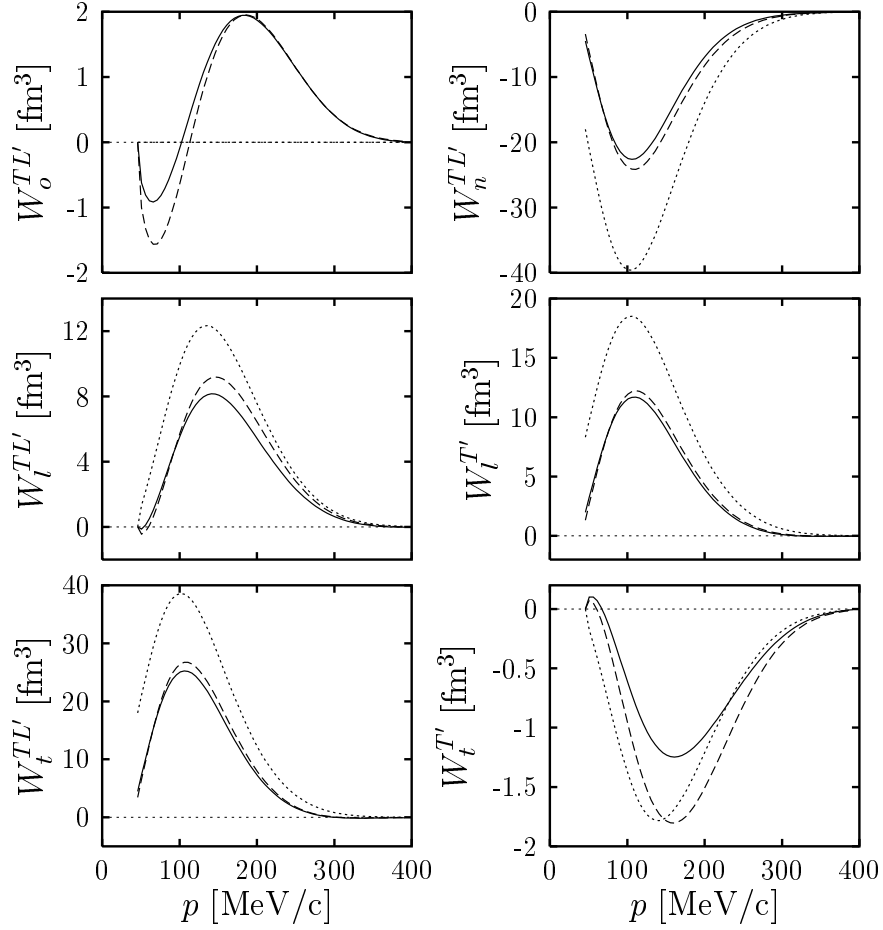


Figure 4: The same as fig. 3 for the fifth and transferred polarized response functions ( $T'$  and  $TL'$ -type responses). With dotted lines we show also for reference the PWIA results.



The five transferred polarized responses which survive in PWIA (61–65), depend less on the details of the potential, being mostly affected by the central imaginary part of it. As known, these responses enter in the case in which also the initial electron is polarized, and they contribute to the transferred nucleon polarization asymmetry. We observe (fig. 4) that both potentials lead to close results, differing by less than 10% for the dominant responses  $W_n^{TL'}$ ,  $W_l^{T'}$  and  $W_l^{TL'}$ , while the largest differences are shown for  $W_t^{T'}$ , which is however very small. Similar results are found for the  $p_{3/2}$  shell. The sensitivity shown by some polarized responses to the details of the potential, makes these observables of special interest to disentangle between the different models of FSI that can fit reasonably well the unpolarized cross sections.

### 3.1.2 Effects of MEC

The impact of MEC on the recoil nucleon polarized responses is shown in Figs. 5–12. In each panel we compare the distorted wave responses evaluated by using the OB current only (dotted line) with the results obtained when including also the two-body MEC operators considered in fig. 2, namely, the seagull or contact (OB+S) current (dashed lines), the contact and pion-in-flight (OB+S+P) currents (dot-dashed lines), and finally, including also the  $\Delta$  current (solid lines), denoted as (OB+MEC). Results in figs. 5–8 correspond to kinematics  $q = 460$  MeV/c,  $\omega = 100$  MeV (kinematics I), whereas in figs. 9–12 we present the responses evaluated at  $q = 1$  GeV/c,  $\omega = 450$  MeV (kinematics II). For both kinematics proton knock-out from the  $p_{1/2}$  (figs. 5,6 and 9,10) and  $p_{3/2}$  (figs. 7,8 and 11,12) have been considered.

Let us discuss first the results for kinematics I (figs. 5-8). Here we observe that the global sign of the polarized  $T$ ,  $TL$  and  $TT$  responses changes when comparing the  $p_{1/2}$  (fig. 5) and  $p_{3/2}$  (fig. 7) shells. The same occurs for kinematics II. Concerning MEC effects, the various polarized responses display different sensitivities to the two-body component of the nuclear current. Apart from the pure longitudinal response  $W_n^L$ , which shows no dependence on MEC because the “semi-relativistic” MEC expressions only include the leading transverse components, the role of MEC on  $W_n^T$  is shown to be similar to the one found for the unpolarized  $T$ -response in [40]: the enhancement (in absolute value) produced by the S current is partially cancelled by the reduction introduced by the P current; the  $\Delta$  current gives rise to an additional reduction, leading to a global decrease of the  $W_n^T$  response of the order of  $\sim 10\%$  at the maximum. This effect being similar for both shells (figs. 5 and 7).

Larger MEC effects are found for some of the induced polarized  $TL$  responses, particularly for  $W_t^{TL}$  where the  $\Delta$  current produces a very significant modification of the response, changing even its shape in the region close to  $p \sim 100$  MeV/c. Note that, although the global effect introduced by the  $\Delta$  in this response is similar for both shells, in the case of the  $p_{1/2}$  there is a large increase, whereas for  $p_{3/2}$  the response is significantly reduced in absolute value. It is also interesting to point out that the  $\Delta$  current plays also

$^{16}\text{O}$ ,  $1p_{1/2}$ ,  $q = 460$  MeV/c,  $\omega = 100$  MeV

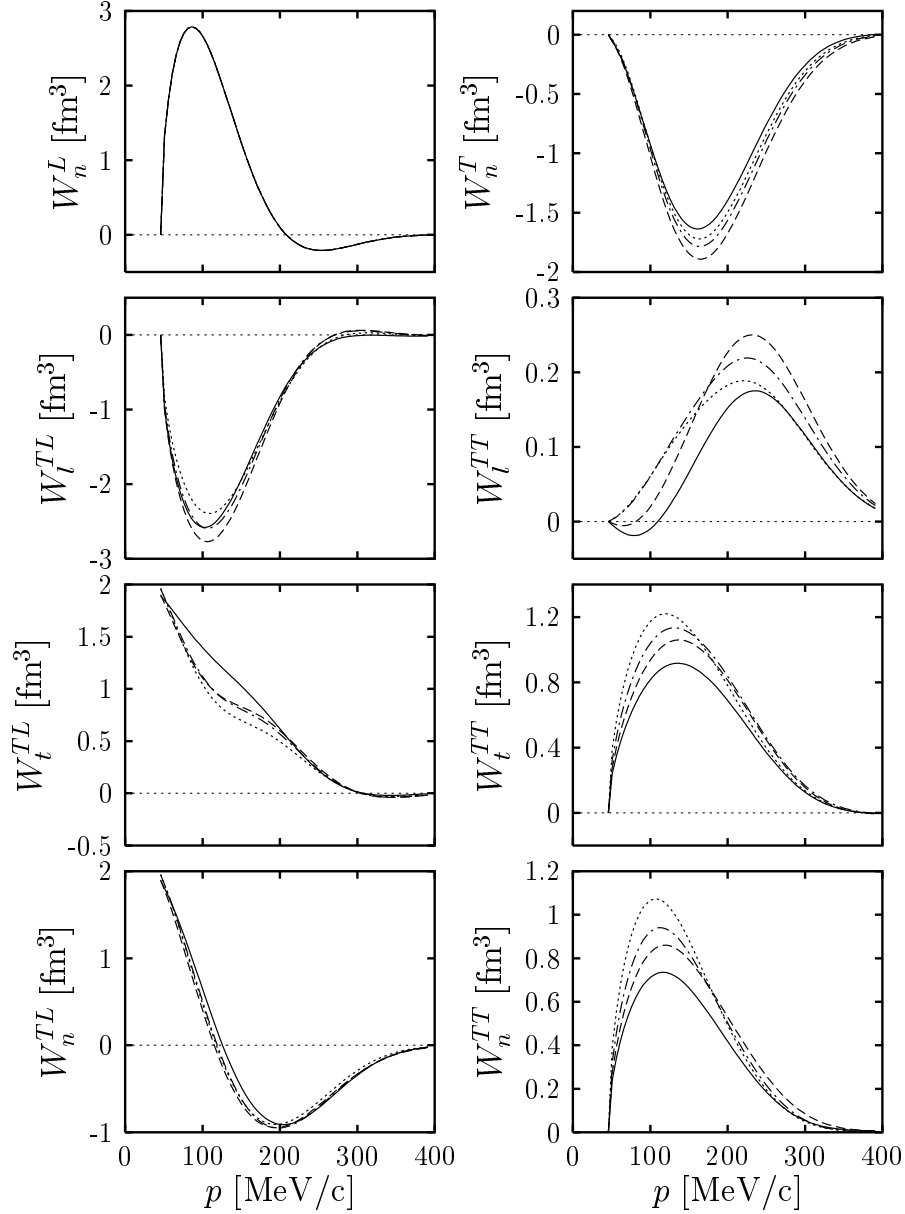


Figure 5: Induced polarized response functions for proton knock-out from the  $1p_{1/2}$  shell in  $^{16}\text{O}$ , with momentum transfer  $q = 460$  MeV/c and energy transfer  $\omega = 100$  MeV. Dotted lines are the DWIA results using only the OB current operator; dashed lines include in addition the seagull current (OB+S); dot-dashed include the seagull plus pionic currents (OB+S+P); finally solid lines represent the total result (OB+MEC) including also the  $\Delta$  current.

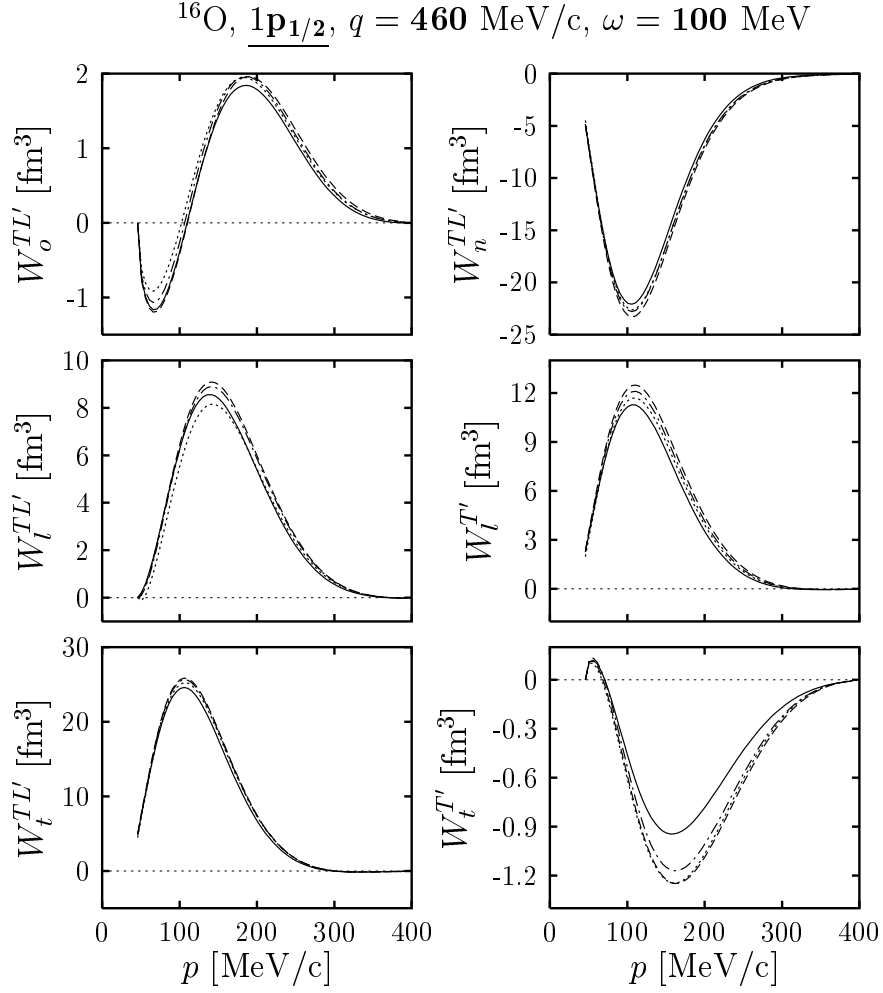


Figure 6: Fifth and transferred polarized response functions for  $^{16}\text{O}$ . Kinematics corresponds to momentum transfer  $q = 460 \text{ MeV}/c$  and energy transfer  $\omega = 100 \text{ MeV}$ . The meaning of the lines is the same as in Figure 5.

the most important role for the  $W_n^{TL}$  response, this being clearly shown in the case of the  $p_{3/2}$  shell.

The role of MEC on the three polarized  $TT$  responses shows a very different behaviour for the two shells considered. In the case of the  $p_{1/2}$  (fig. 5), the global effect of MEC is a very significant reduction of the responses, particularly for  $W_t^{TT}$  ( $\sim 20\%$ ) and  $W_n^{TT}$  ( $\sim 30\%$ ), being the separate contributions of the S, P and  $\Delta$  currents of rather similar importance. Note that the contributions introduced by the S and P currents have opposite signs for the  $p_{1/2}$  and  $p_{3/2}$  shells. As a consequence, for the  $p_{3/2}$  shell (fig.7) the large enhancement (in absolute value) produced by the S current is almost cancelled exactly by the contributions of the P and  $\Delta$  currents, so the net MEC effect is almost negligible for the three  $TT$  responses.

The transferred polarized responses ( $T'$  and  $TL'$ -type responses) are shown in Figs. 6 and 8. From these results we find in general a small effect of MEC, less than  $\sim 5\%$ . An exception is  $W_t^{T'}$  where the role of  $\Delta$  gives rise to an important reduction of the response; however notice that  $W_t^{T'}$  is very small, of the order of  $\sim 10\%$  compared with  $W_l^{T'}$  and  $W_t^{TL'}$ , and hence difficult to measure. The anomalous smallness of the response  $W_t^{T'}$  was already discussed in detail in [31] within the context of the PWIA and different non-relativistic reduction schemes. This result can be also understood within the multipole analysis performed in this work by taking into account the general relations given in eqs. (49,50) and the explicit expressions obtained for the multipole functions in PWIA (61,62). Since we are close to the quasielastic-peak, the angle  $\theta'$  is close to zero for moderate missing momentum, so the biggest contribution comes from the factor multiplied by  $\cos \theta'$  in eqs. (49,50). This factor is  $W_{10}^K = O(1)$  in the case of the  $l$ -responses, and  $W_{11}^K = O(\chi)$  for the  $t$ -response. Precise values of the nucleon form factors and kinematical variables can be introduced in these equations to verify the exact relation between the  $l$  and  $t$  components in PWIA, which is not very different from the distorted-wave results of figs. 6 and 8.

Results for higher momentum and energy transfer,  $q = 1000$  MeV/ $c$  and  $\omega = 450$  MeV (kinematics II), are shown in Figs. 9–12 for the two  $p$  shells in  $^{16}\text{O}$ . This kinematics corresponds to the experimental setting of [16, 22] where  $Q^2 = -0.8$  (GeV/ $c$ ) $^2$ . Obviously in this case relativity is expected to play a more important role and in fact, studies within the relativistic distorted wave impulse approximation (RDWIA) [13] have proved the importance of these effects. The present SR model, although lacking some of the relativistic ingredients inherent in the RDWIA, incorporates exact relativistic kinematics for the ejected nucleon, a SR expansion of the current which can be used for high  $q$  values, and finally, the use of the Schrödinger-equivalent form of the S-V Dirac global optical potential of [54], including the Darwin term in the wave function. The validity of the expansion procedure used in the SR model was tested in [13] where unpolarized observables evaluated within the SR approach were compared with a RDWIA calculation for this kinematics.

The discussion of the results presented in figs. 9-12 follows similar trends to the ones already presented for kinematics I, so here we simply summarize those aspects which can

$^{16}\text{O}$ ,  $1p_{3/2}$ ,  $q = 460$  MeV/c,  $\omega = 100$  MeV

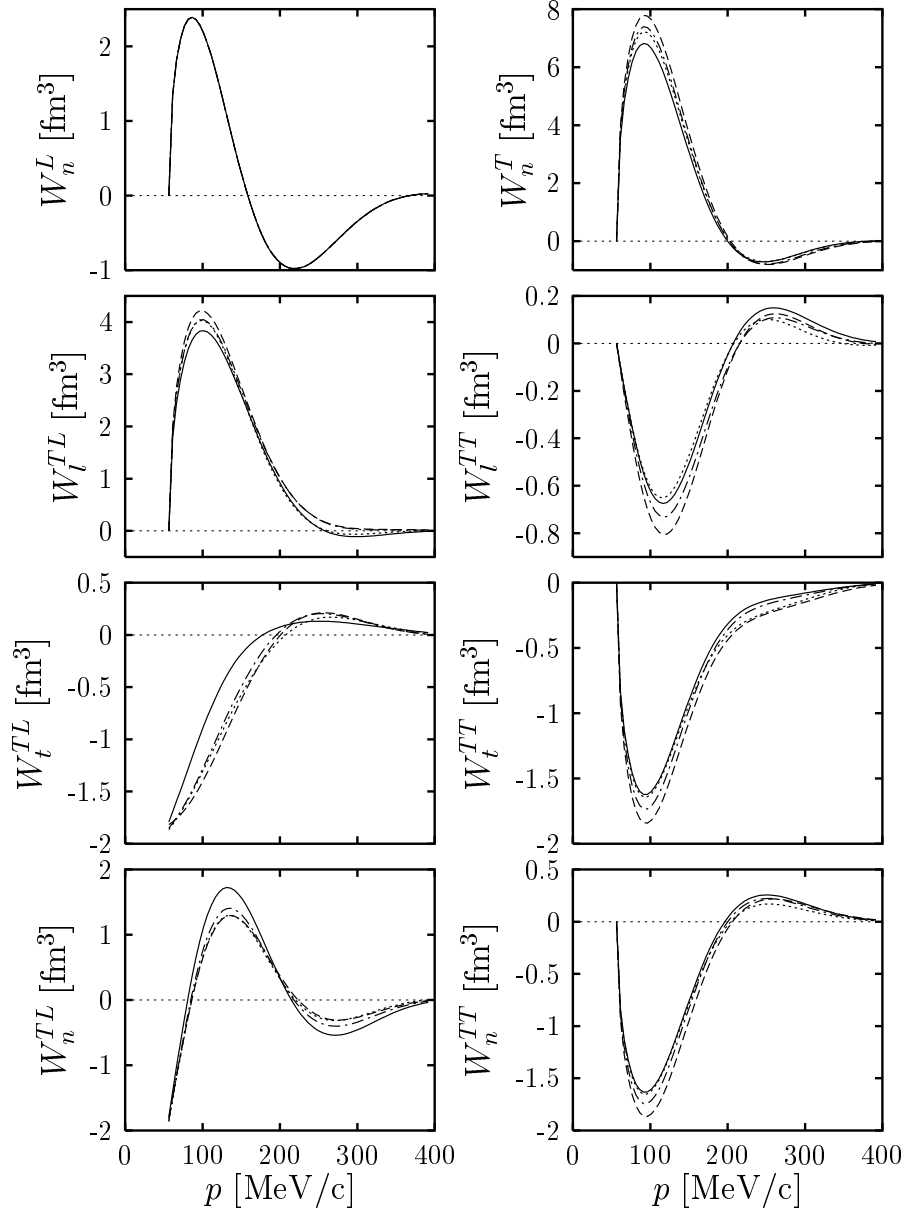


Figure 7: The same as Fig. 5 for proton knock-out from the  $1p_{3/2}$  shell.

$^{16}\text{O}$ ,  $\underline{1p_{3/2}}$ ,  $q = 460$  MeV/c,  $\omega = 100$  MeV

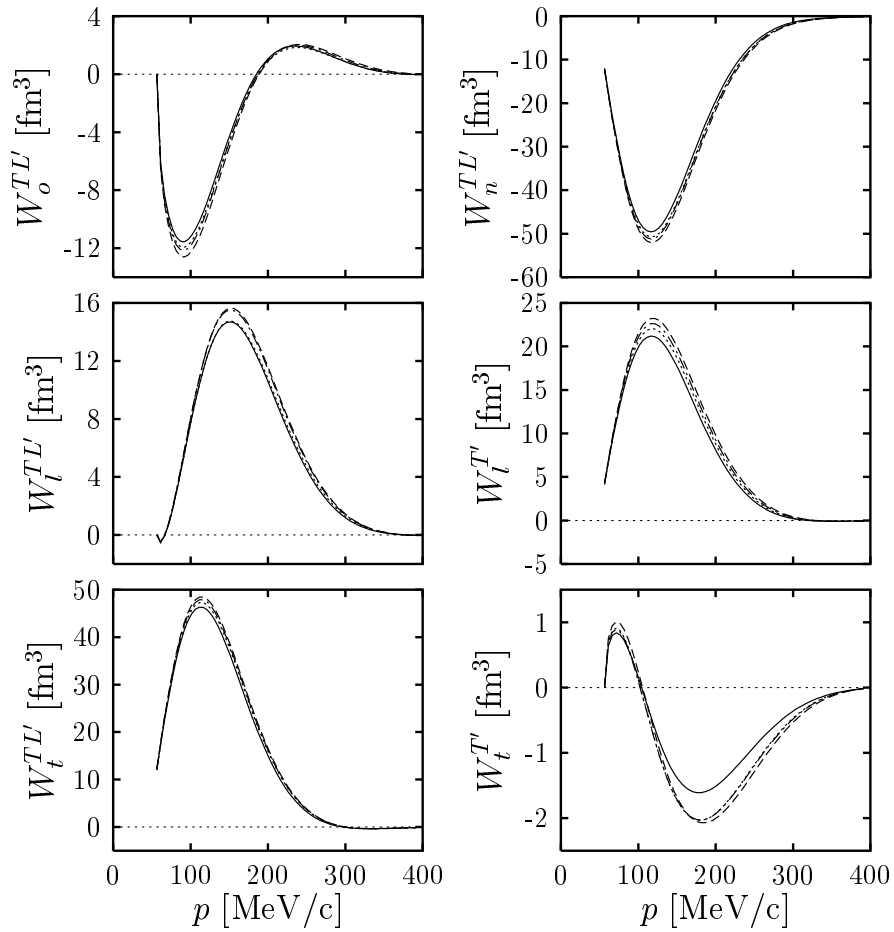


Figure 8: The same as Fig. 6 for proton knock-out from the  $1p_{3/2}$  shell.

$^{16}\text{O}$ ,  $\underline{1p_{1/2}}$ ,  $q = 1000$  MeV/c,  $\omega = 450$  MeV

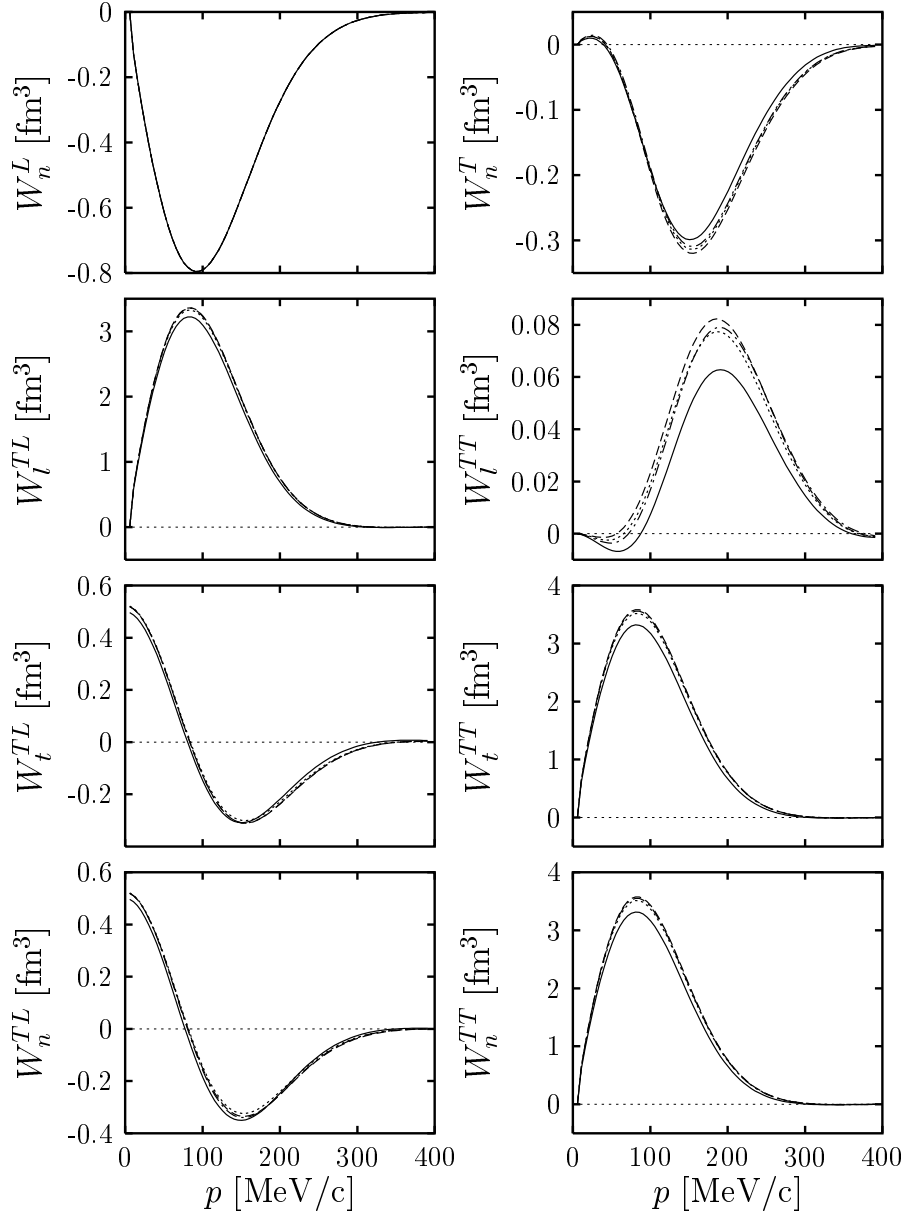


Figure 9: The same as Fig. 5 for  $q = 1000$  MeV/c and  $\omega = 450$  MeV.

$^{16}\text{O}$ ,  $\underline{1p_{1/2}}$ ,  $q = 1000$  MeV/c,  $\omega = 450$  MeV

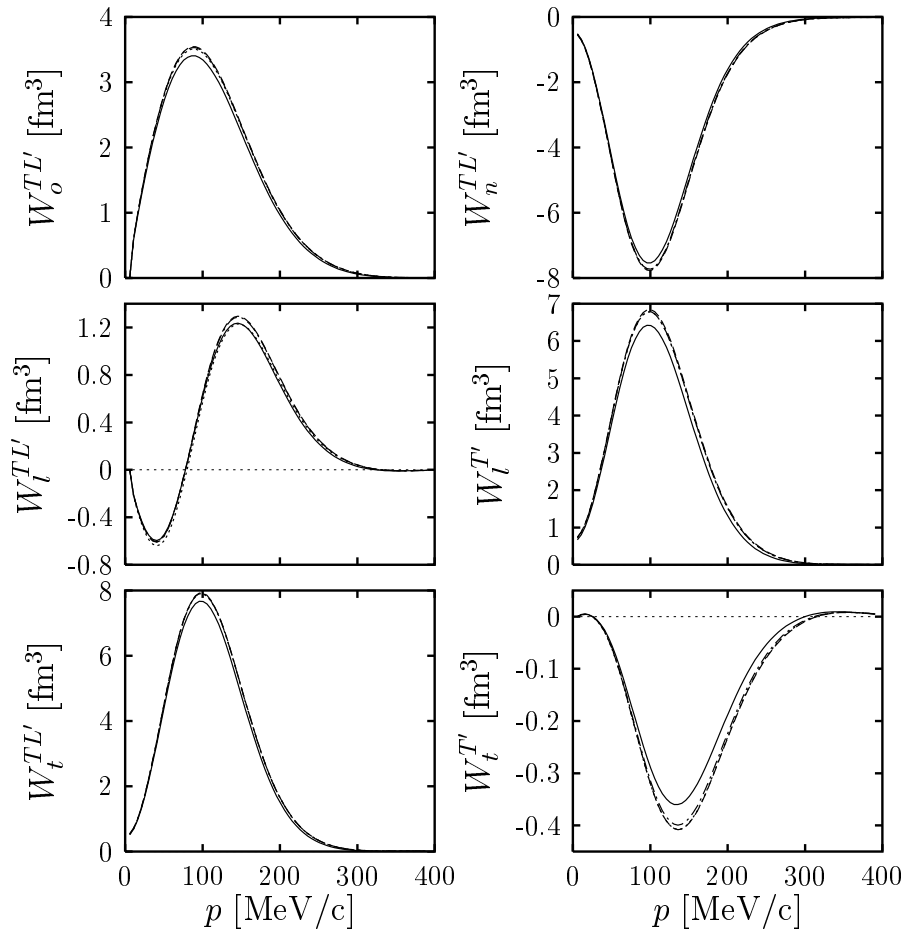


Figure 10: The same as Fig. 6 for  $q = 1000$  MeV/c and  $\omega = 450$  MeV.



$^{16}\text{O}$ ,  $1p_{3/2}$ ,  $q = 1000$  MeV/c,  $\omega = 450$  MeV

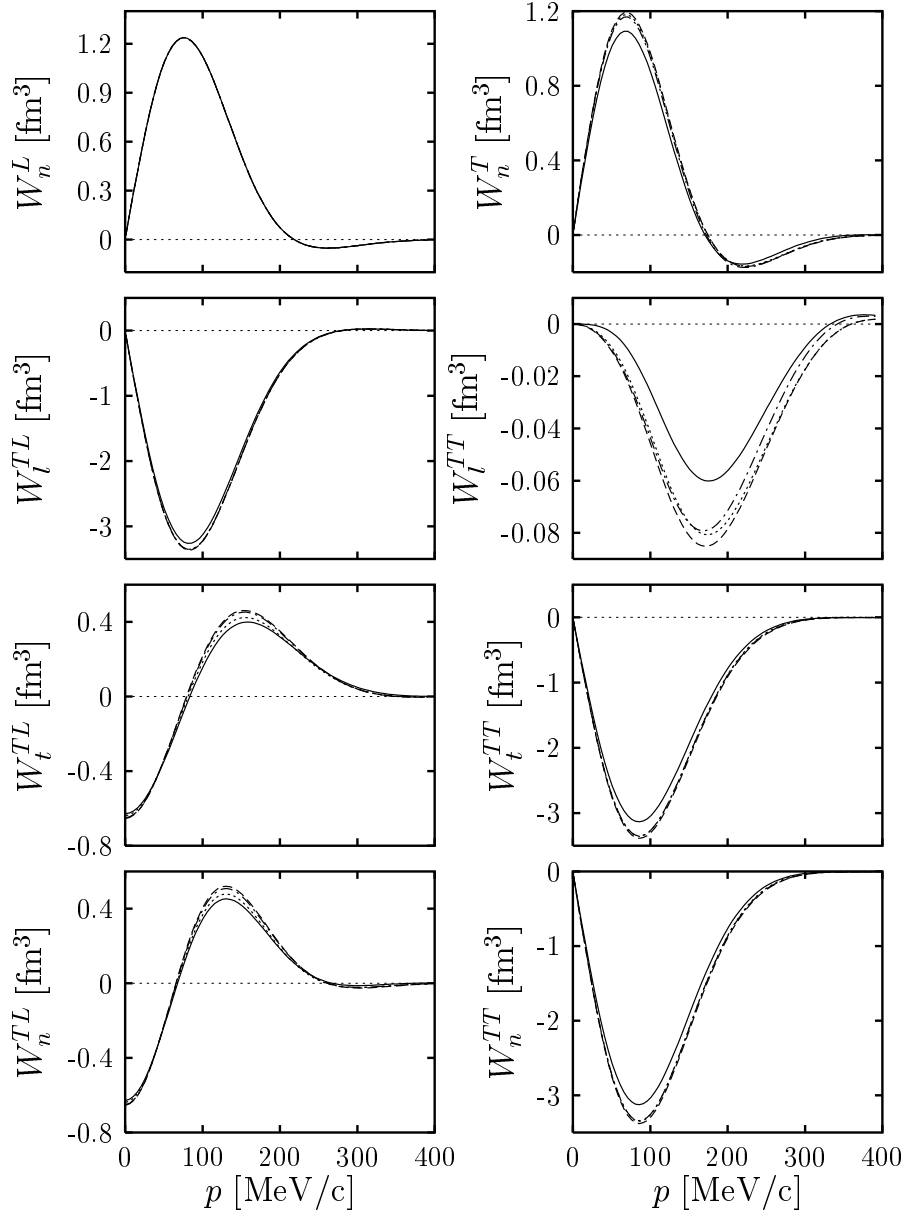


Figure 11: The same as Fig. 5 for the  $p_{3/2}$  shell,  $q = 1000$  GeV/c, and  $\omega = 450$  MeV.

$^{16}\text{O}$ ,  $\underline{1p}_{3/2}$ ,  $q = 1000$  MeV/c,  $\omega = 450$  MeV

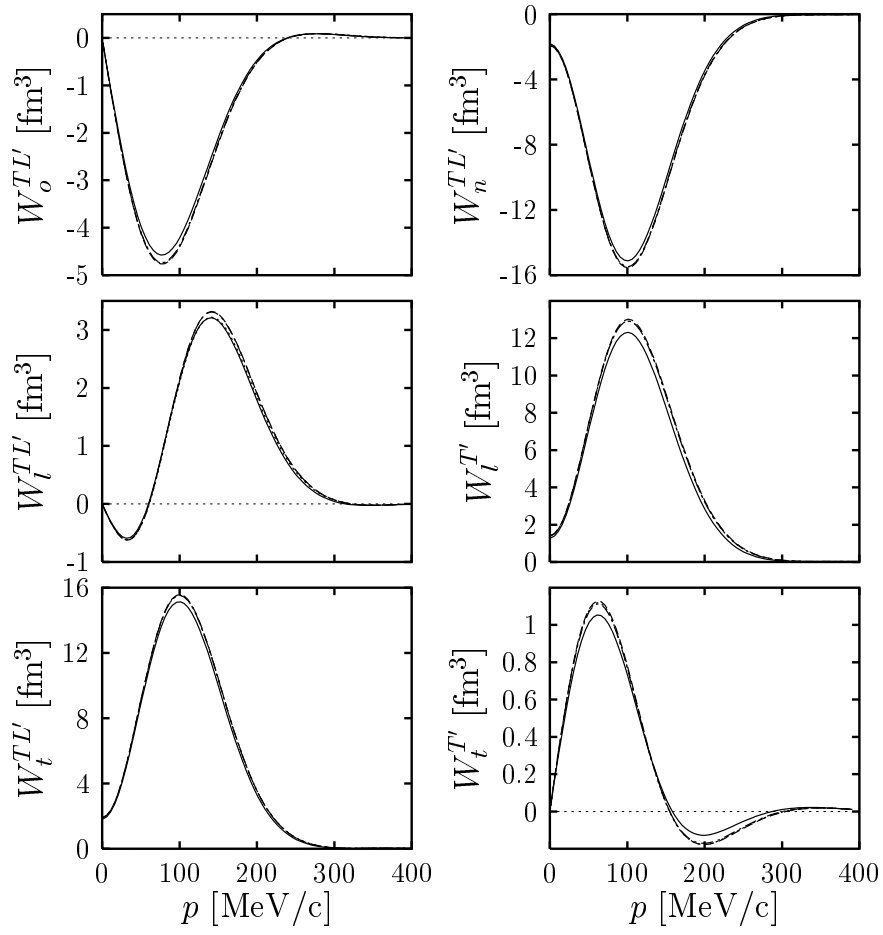


Figure 12: The same as Fig. 6 for the  $p_{3/2}$  shell,  $q = 1000$  MeV/c and  $\omega = 450$  MeV.

be of more relevance. As shown in figs. 9-12, the general effect introduced by MEC is a global reduction of the responses (in absolute value) whose magnitude depends on the specific response, being of the order of a few percent for  $W_{l,t,n}^{TL}$  and  $W_{0,l,t,n}^{TL'}$ , larger for  $W_n^T$ ,  $W_{t,n}^{TT}$  and  $W_{l,t}^{T'}$  (particularly because of the  $\Delta$ -contribution) and the largest for  $W_l^{TT}$ , where the reduction (basically due to  $\Delta$ ) is about  $\sim 20 - 25\%$ . Note however that the response  $W_l^{TT}$  is the smallest one and so hardly measurable.

The dependence of MEC effects on the momentum transfer shown in the results of figs. 5–12 is consistent with the findings of ref. [40] for the unpolarized responses. In general the importance of MEC decreases with  $q$ . This is in accord with the results for the  $T$  response in the  $1p - 1h$  channel in the case of quasielastic inclusive ( $e, e'$ ) reactions [45, 46]. This behaviour can be roughly understood from the relativistic expressions for the particle-hole transverse current matrix elements  $\mathbf{J}_T(\mathbf{p}', \mathbf{p})$  in Fermi gas [45, 46], and also from the traditional non relativistic expressions. At the non relativistic level, the OB current is dominated by the magnetization contribution which goes as  $\sim q$ . On the contrary, MEC present a much more complex dependence on  $q$  and on the momenta of the two holes involved: the missing momentum  $\mathbf{p}$  and an intermediate momentum  $\mathbf{k}$  which should be integrated. Moreover, MEC also contain pion propagators involving inverse squared pion momenta. For high  $q$ , a crude estimation of the (transverse) seagull and pion in flight currents is shown to behave as  $\sim q/(q^2 + m_\pi^2)$ , while the  $\Delta$  current goes as  $\sim q^3/(q^2 + m_\pi^2)$ , hence the latter clearly dominates, which is in accord with the results shown here. Once the  $\pi N$  form factor, which becomes smaller when high momenta are probed, is added to the two-body currents, we find the OB contribution to dominate over the MEC. At the relativistic level the above dependences on  $q$  change. In [44] it was demonstrated that if the form factors are neglected, then the OB, seagull and pionic currents grow asymptotically as  $\sqrt{q}$ . Thus the inclusion of  $\pi N$  form factors is essential for the dominance of the OB current. This conclusion however applies to the response functions only for low missing momentum, since for other observables such as the  $A_{TL}$  asymmetry [40] and the polarization asymmetries (see below) larger effects are found for high values of  $q$  and missing momentum.

### 3.2 Transferred polarization asymmetries

Apart from the response functions, other observables of special interest are the nucleon polarization asymmetries introduced in eqs. (18-21). These observables are given as ratios between polarized and unpolarized responses, where one hopes to gain different insight into the underlying physics from what is revealed through the responses themselves. As already mentioned in the introduction and in order to clarify the discussion, here we restrict ourselves to the analysis of the transferred polarization asymmetries  $P'_{l,t,n}$ , which only enter with polarized incident electrons and persist in PWIA. Induced polarization ratios  $P_{l,t,n}$  —that do not depend on the polarization of the incident electron and are zero within the plane wave approach—, and total cross sections will be analyzed in a forthcoming publication [51].

Following the discussion presented for the responses, here we first study the effects introduced by FSI and later on we focus on the role of MEC.

### 3.2.1 Effects of FSI

In Figs. 13–14 we present the results obtained for the transferred polarization asymmetries corresponding to proton knockout from the  $p_{1/2}$  and  $p_{3/2}$  shells in  $^{16}\text{O}$ . Kinematics has been selected as (I), i.e.,  $q = 460$  MeV/c and  $\omega = 100$  MeV. Results for kinematics (II) follow the same general trends although FSI effects are in general less important because of the higher momentum transfer involved. The longitudinal  $P'_l$  and transverse (sideways)  $P'_t$  components are shown in fig. 13 for electron scattering angle fixed to  $\theta_e = 30^\circ$  (forward scattering) and three values of the proton azimuthal angle  $\phi = 0, 90^\circ$  and  $180^\circ$ , while the normal polarization  $P'_n$  is displayed in fig. 14 for  $\phi = 90^\circ$  (notice that  $P'_n$  is zero for co-planar kinematics). Although not shown here for brevity, we have also explored the behaviour of the transferred polarization ratios at backward scattering angle ( $\theta_e = 150^\circ$ ). As known, the purely transverse responses dominate at backward angles, whereas all of the kinematical factors that enter in the description of  $(\vec{e}, e'\vec{p})$  reaction are of similar order at forward angles. In [30] forward scattering angles were proved to enhance significantly the sensitivity to dynamical relativistic effects. Concerning FSI and MEC, the discussion of the results for  $\theta_e = 150^\circ$  follow similar trends to the ones presented here for  $\theta_e = 30^\circ$ .

The PWIA calculation (dotted line) is compared with DWIA results using the two optical potentials already presented in the previous section, i.e., Comfort & Karp (solid lines) and Schwandt (dashed lines). First, notice the difference between PWIA and DWIA results. Within the plane wave approach, the responses factorize and hence the polarization ratios depend only on the single-nucleon responses, being cancelled the whole dependence with the momentum distribution. This means that PWIA results are identical for the two  $p$ -shells considered. Moreover, polarization ratios in PWIA may be written in the general form

$$P'_i = \frac{a_i + b_i\chi + O(\chi^2)}{c_i + d_i\chi + O(\chi^2)}, \quad \text{for } i = l, t, n, \quad (66)$$

where  $\chi = p/m_N \sin \theta$ , already introduced in (51-53), is the parameter in the SR expansion of the nuclear current. For low missing momentum, the above fraction has a linear dependence on  $\chi$  plus a small correction of order  $\chi^2$  which breaks linearity for higher  $p$ .

For low missing momentum values  $p \leq 200$  MeV/c, the effects introduced by FSI are small, being almost negligible at the maximum of the momentum distribution ( $p \approx 100$  MeV/c). This result is expected because of the global reduction of the polarized response functions produced by FSI: of the order of  $\sim 30\%$  (fig. 4). This is somewhat similar to the behaviour shown by the unpolarized responses [38]. Hence, although not exact because

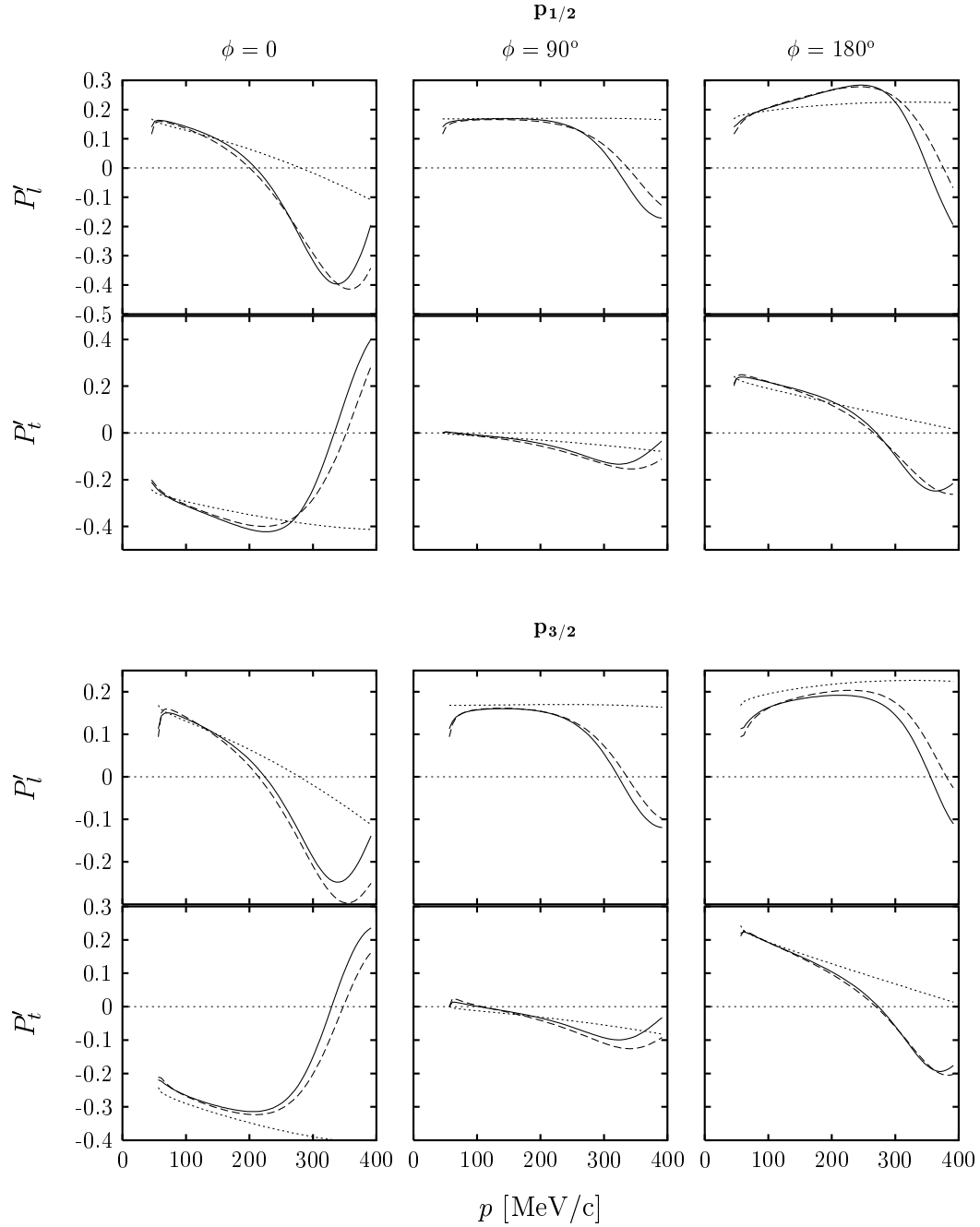


Figure 13: Transferred polarization ratios  $P'_l$  and  $P'_t$  for proton knock-out from the  $p$  shells in  $^{16}\text{O}$ , and  $q = 460$  MeV/c,  $\omega = 100$  MeV. The electron scattering angle is  $\theta_e = 30^\circ$ , and results are shown for three values of the proton azimuthal angle  $\phi = 0, 90^\circ, 180^\circ$ . Solid lines have been computed in DWIA with the Comfort and Karp potential, dashed lines with the Schwandt potential, and finally the dotted lines are the PWIA results.

of the slightly different sensitivities to FSI shown by the various responses, a kind of cancellation of FSI between the numerator and denominator in the polarization ratios occurs for low  $p$ . From results in fig. 13, one also observes that FSI effects are slightly bigger in the case of the  $p_{3/2}$  shell, particularly for  $P'_l$  and  $\phi = 180^\circ$ . The reason of this is connected to the much less reduction that FSI cause upon the unpolarized  $TL$  response for  $p_{3/2}$  (see [38] for details).

For high missing momentum the DWIA polarizations deviate significantly from the PWIA results, showing a very pronounced oscillatory behavior which may even give rise to a change of sign in the polarizations. This is a clear indication that for high momentum the effects of FSI are not simply a global reduction of the responses due to the imaginary part of the potential, but on the contrary, each response turns out to present a peculiar sensitivity to the interaction. As shown in figs. 3 and 4, this is hardly visible in the separate response functions because of the smallness of the momentum distribution for high  $p$ . It is important to point out that the oscillatory behaviour presented by the polarization ratios is a direct consequence of the breaking of factorization property. This issue was already studied at the level of the plane wave approach taking care of the dynamical relativistic effects introduced by the lower components of the bound Dirac spinors [30]. A general analysis of factorization within the context of the RDWIA and different non-relativistic approximations is presently in progress [32].

Focusing on the results presented in fig. 13, we observe that the shape and magnitude of both polarization asymmetries,  $P'_l$  and  $P'_t$ , are similar for the two  $p$ -shells. In the particular case of  $\phi = 90^\circ$  (out-of-plane kinematics) the ratio  $P'_t$  is very small, almost negligible for low missing momentum. This is expected since only the response  $W_t^{T'}$ , which is very small, contributes to  $P'_t$  in that situation. For co-planar kinematics a large discrepancy between the results obtained at  $\phi = 0^\circ$  and  $\phi = 180^\circ$  exists. As shown by eqs. (13–16), the numerator in the ratios  $P'_i$ ,  $i = l, t$ , is given through the linear combination  $v_{T'}W_i^{T'} + v_{TL'}W_i^{TL'} \cos \phi$ , with the kinematical factors being  $v_{T'} = 0.27$  and  $v_{TL'} = -0.18$  for the kinematics considered here (I). Hence, from the transferred polarization asymmetries measured at  $\phi = 0^\circ$  and  $\phi = 180^\circ$ , the separate responses  $W_i^{T'}$  and  $W_i^{TL'}$  could be extracted.

Comparing the solid and dashed lines in fig. 13 we conclude that the uncertainties introduced by the optical potentials selected are rather small. For low momentum transfer these differences are negligible in contrast to fig. 4 where some responses are shown to be affected appreciably by the optical potential. This again is an outcome of the fact that the differences between the responses computed with these potentials are of the same size in numerator and denominator and they tend to cancel when taking the quotient to compute the polarizations. Both sets of results start to differ for  $p \geq 300$  MeV/c. Note however that for high  $p$ -values other relativistic effects coming from the dynamical enhancement of the lower components in the wave functions, not included in the present model, may also contribute significantly to the oscillatory behaviour of the polarizations [30, 32].

The case of the normal polarization transfer  $P'_n$  (fig. 14), present some peculiarities not observed for  $P'_{l,t}$ . First the difference between PWIA and DWIA results is rather constant

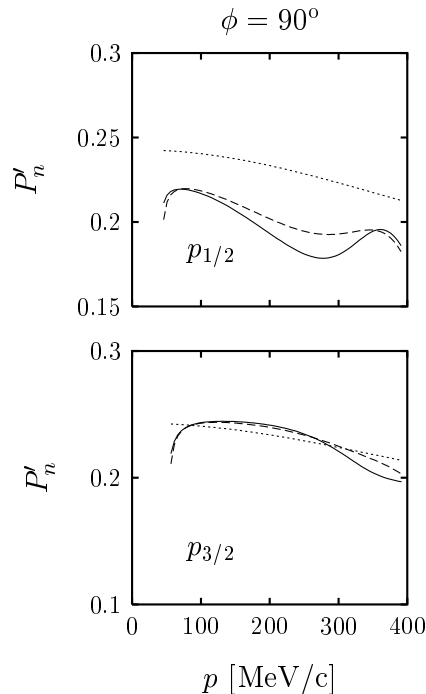


Figure 14: The same as Fig. 13 for the polarization transfer component  $P'_n$  and  $\phi = 90^\circ$ .

for the two shells in the whole range of missing momentum. In particular, the distorted wave approach leads to results which are very similar to the ones obtained within PWIA in the case of the  $p_{3/2}$ . In addition, the strong oscillatory behaviour due to FSI and shown for  $P'_{l,t}$  (fig. 13) does not appear here, being the differences introduced by both optical potentials small. These results could promote this observable  $P'_n$ , that can be obtained in out-of-plane experiments, as a good candidate in order to study properties of the reaction without being much affected by FSI.

### 3.2.2 Effects of MEC

In Figs. 15–17 we present the effects introduced by MEC upon the transferred proton polarization components for the two  $p$  shells in  $^{16}\text{O}$ , and for the two kinematics considered above. In the case of kinematics (I), i.e.,  $q = 460$  MeV/c (fig. 15), where we use the optical potential parameterized by Comfort & Karp, MEC effects are shown to be small in the whole missing momentum range and similar for both shells. Note also that the role played by MEC is of the same order of magnitude or even smaller than the uncertainty introduced by the use of the two optical potentials (fig. 13). The smallness of MEC effects on the polarization asymmetries comes from their effective cancellation when taking ratios of response functions.

Results for higher momentum transfer,  $q = 1000$  MeV/c (kinematics II), are shown in Fig. 16 for the Schrödinger-equivalent form of the S-V Dirac global optical potential of ref. [54]. As in the previous case, MEC effects are small for low missing momentum; however they tend to increase significantly for higher  $p$ -values due to the  $\Delta$  exchange current, inducing a softening of the transferred polarization asymmetry, which makes its oscillatory behaviour to appear at slightly lower momenta (see for instance the important MEC effects observed for  $P'_l$  at  $\phi = 0$ , particularly in the region close to the minimum  $p \sim 300$  MeV/c). The present results indicate that the response functions entering into the polarization ratios are importantly affected by MEC, mainly due to the  $\Delta$  current, for high momentum transfer. Large effects of this kind have also been found recently for the  $A_{TL}$  asymmetry obtained from the analysis of unpolarized (e,e'p) reactions corresponding to the same kinematics II [40].

The normal polarization  $P'_n$  is shown in Fig. 17 for the two kinematics and both shells. MEC effects follow the same trends as those observed for  $P'_l$  and  $P'_t$ : they increase significantly for high momentum transfer ( $q = 1000$  MeV/c) and high missing momentum. In contrast with the  $P'_l$  and  $P'_t$  cases, here the relative contributions of the separate MEC currents depend on the specific kinematics and  $p$ -shell selected, playing the seagull and pion-in-flight currents an important role.

To finish we present in Fig. 18 the asymmetries  $P'_l$  and  $P'_t$  evaluated for  $q = 1000$  MeV/c,  $\omega = 450$  MeV and electron incident energy  $\epsilon_e = 2450$  MeV. This kinematics corresponds to a recent experiment performed at TJlab. We compare our calculations with the experimental data presented in [22]. The azimuthal angle in this experiment was  $\phi = 180^\circ$ . Note the change of sign of  $P'_t$  with respect to the results of Fig. 16, due to the opposite definitions of the normal plane (and hence of the  $t$  component) for  $\phi = 180^\circ$  (in our case the normal plane for  $\phi = 180^\circ$  would point down in Fig. 1, while in ref. [22] it was chosen along the up direction). Results for the  $p$  and  $s$  shells in  $^{16}\text{O}$  are shown from left to right. Although being aware of the possible modifications that the “dynamical” relativistic ingredients [13, 27, 22] may introduce in the present calculations, we are rather confident that the results in fig. 18 give us a clear indication of how much the DWIA calculation is expected to be modified after including the two-body (MEC) contributions (compare dotted with solid lines). As noted, whereas the contribution of MEC over  $P'_t$  is negligible, they give rise to a slight reduction of  $P'_l$ , which is well inside the experimental error except for the  $s_{1/2}$  shell. Comparing the results for the two  $p$ -shells we observe that our model describes better the case of the  $p_{3/2}$ . This is in agreement with the findings in [13, 40] concerning the  $A_{TL}$  asymmetry. The particular case of  $s_{1/2}$  shows that the experimental data for  $P'_t$  are well reproduced by the calculations, which however underestimate very significantly the data for  $P'_l$ .

In order to clarify the importance of FSI, in fig. 18 we also show with dot-dashed lines the results corresponding to the global OB+MEC calculation but without including the spin-orbit term of the optical potential, i.e., using a phenomenological optical potential consisting only of a central part. As shown, the corresponding polarizations present some



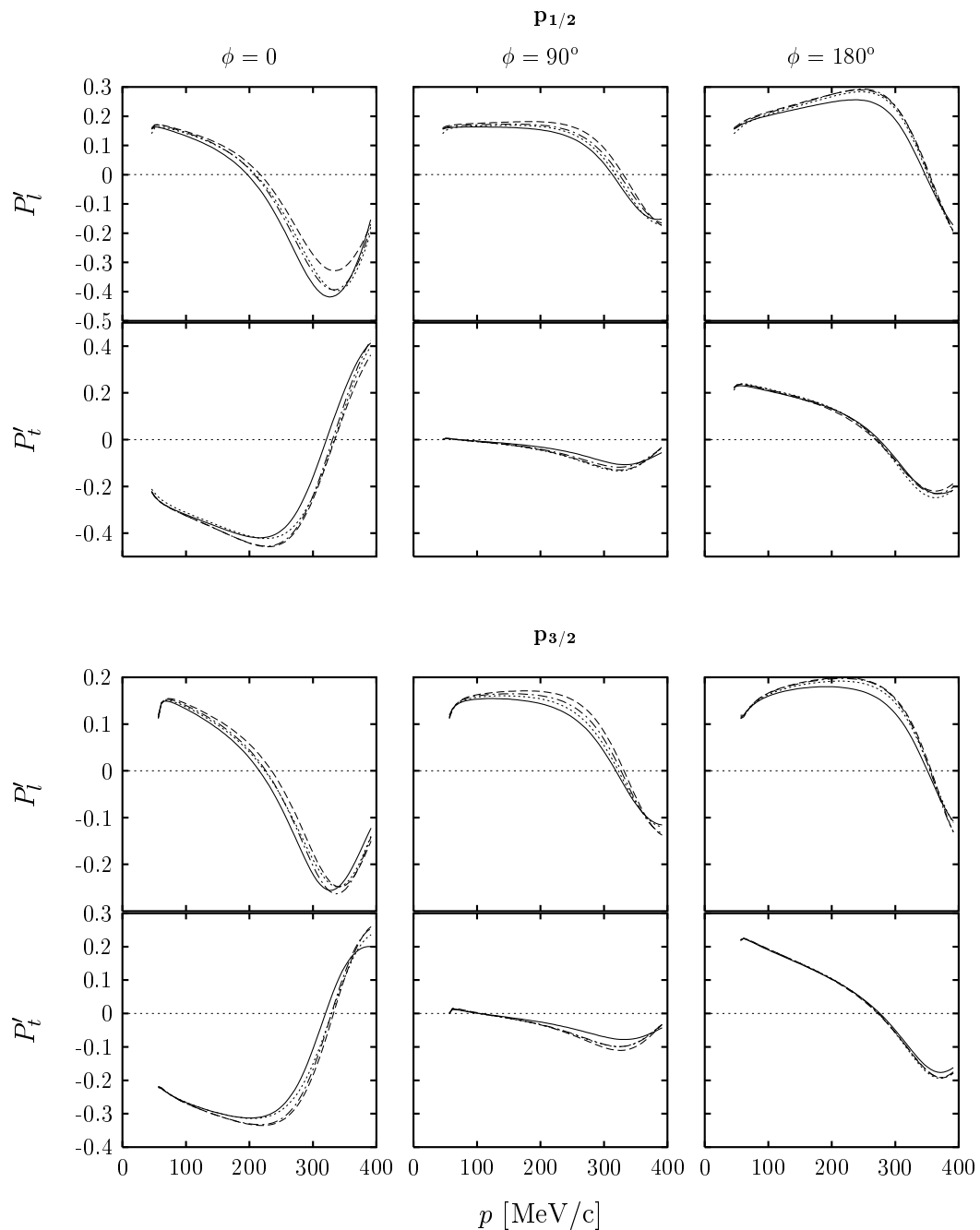


Figure 15: MEC effects over the transferred polarization asymmetries  $P'_l$  and  $P'_t$  for proton knock-out from the  $p$  shells in  $^{16}\text{O}$ , and  $q = 460$  MeV/c,  $\omega = 100$  MeV. The electron scattering angle is  $\theta_e = 30^\circ$ , and results are shown for three values of the proton azimuthal angle  $\phi = 0, 90^\circ, 180^\circ$ . The meaning of the lines is the same as in Fig. 5.

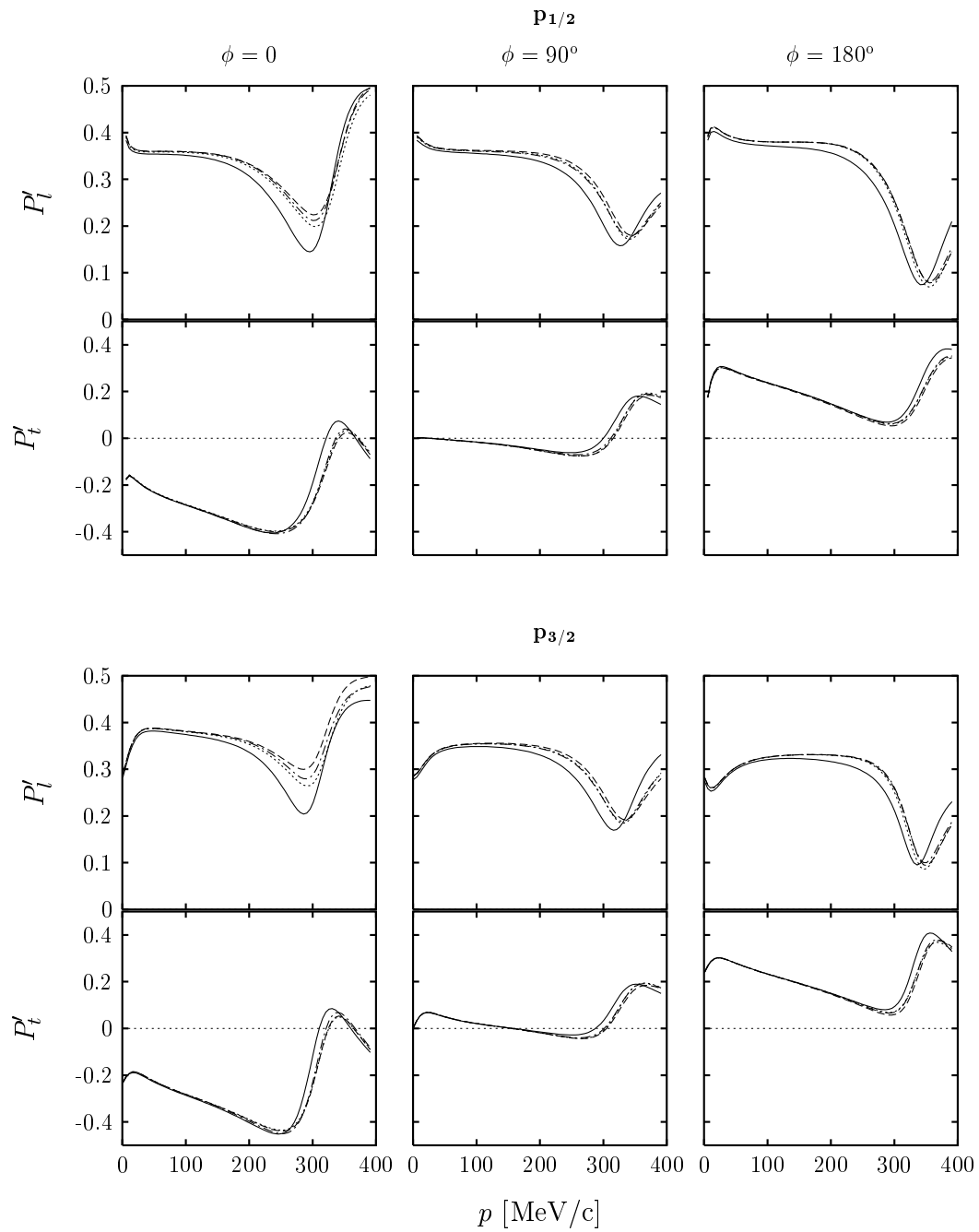


Figure 16: The same as Fig. 15 for  $q = 1000$  MeV/c and  $\omega = 450$  MeV.

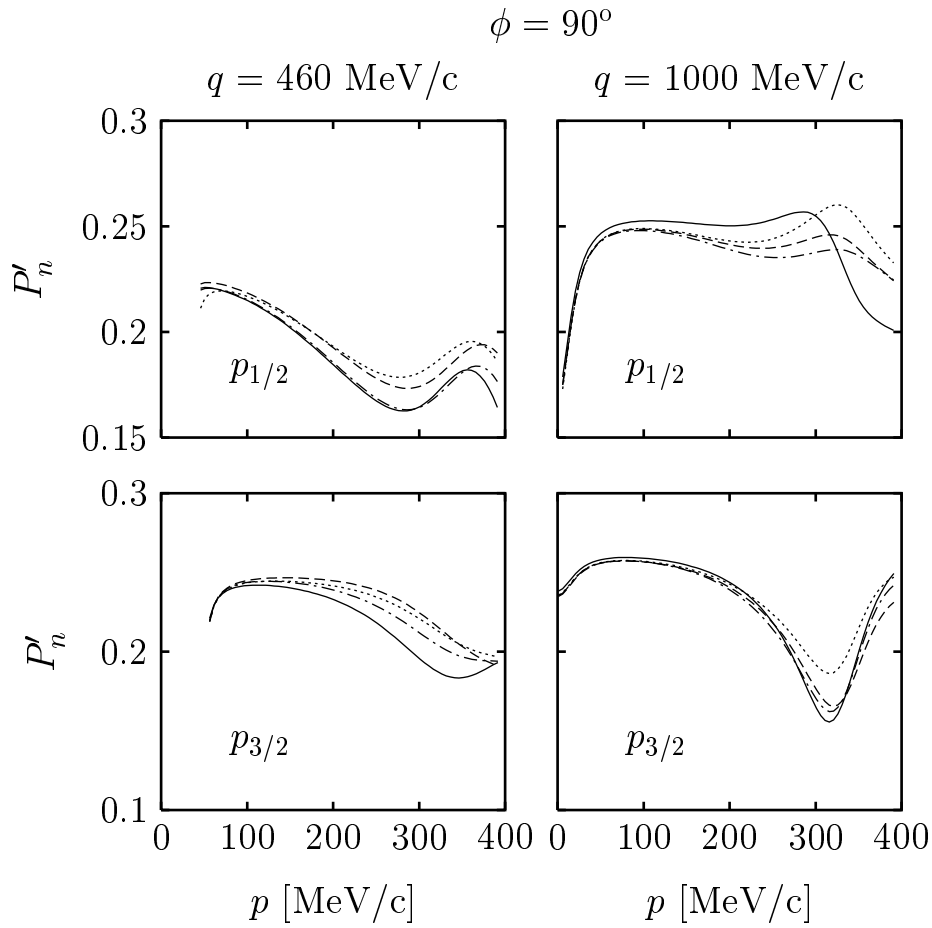


Figure 17: The same as Figs. 15 and 16 for the normal polarization transfer component  $P'_n$  and  $\phi = 90^\circ$ .

kind of “linearity”, being similar to the PWIA results. This is expected since the spin-orbit interaction is the main responsible of the oscillatory behaviour of the polarization ratios, apart from the “dynamical” relativistic effects.

The ratio  $P'_t/P'_l$ , shown in the bottom panels of fig. 18, has been proposed as a suitable observable for getting information on nucleon properties inside the nuclear medium [55]. From inspection of fig. 18 we find that MEC produce a tiny reduction of this observable, particularly for low missing momentum, being larger as  $p$  goes up.

All of the above results have been computed using the Galster parameterization for the nucleon form factor. It is of interest to know the dependence of our results with the nucleon structure, hence we have also calculated the OB+MEC polarization asymmetries assuming the Gari-Krumplemann (GK) form factor parameterization [56]. The results are shown with dashed lines. The GK parameterization was used by Udias et al. [57] within the context of the relativistic calculations presented in ref. [22]. The  $P'_l$  computed with GK form factors is increased with respect to the solid lines, being a little bit closer to the experimental data. Let us remind that the effects of MEC lead to a global reduction of all of these polarization observables, hence the OB calculation using the GK form factors would be clearly located above the corresponding results including MEC (dashed lines). This makes our present results to come closer to the relativistic ones of [22]. Note also that the uncertainty introduced by the nucleon form factor parameterization shows up in  $P'_l$ , being negligible for  $P'_t$ .

To finish the discussion, it is also interesting to point out that the behaviour shown by the  $P'_t$  data, growing with  $p$  for  $p_{1/2}$  and the reverse for  $p_{3/2}$ , does not agree with the theoretical results which increase with  $p$  for both shells. This is in accordance with other relativistic calculations [22]. For  $p = 140$  MeV/c our predictions for  $P'_t$  in the case of the  $p_{1/2}$  shell clearly underestimate the data; as already mentioned, other relativistic effects coming from the lower components of the Dirac wave functions, not considered here, may also play a significant role.

### 3.3 Comparison with previous works

Concerning previous calculations of MEC in  $(e, e'p)$  reactions, in [38, 40] comparisons for unpolarized observables obtained with the present model with those of Refs. [34, 35, 37, 39] were presented. Next we summarize the differences of MEC effects on recoil polarization observables between the present work and Refs. [33, 36].

1. Boffi and collaborators [33] find for intermediate  $q$  values large MEC effects on the separate polarized responses (reduction of the order of 15-30% or even larger), being the  $\Delta$  current the main contribution. We get in general smaller and qualitatively different effects for this kinematics, the seagull and pion in flight currents being in our case as important as the  $\Delta$ . Concerning the transfer polarization ratios, they

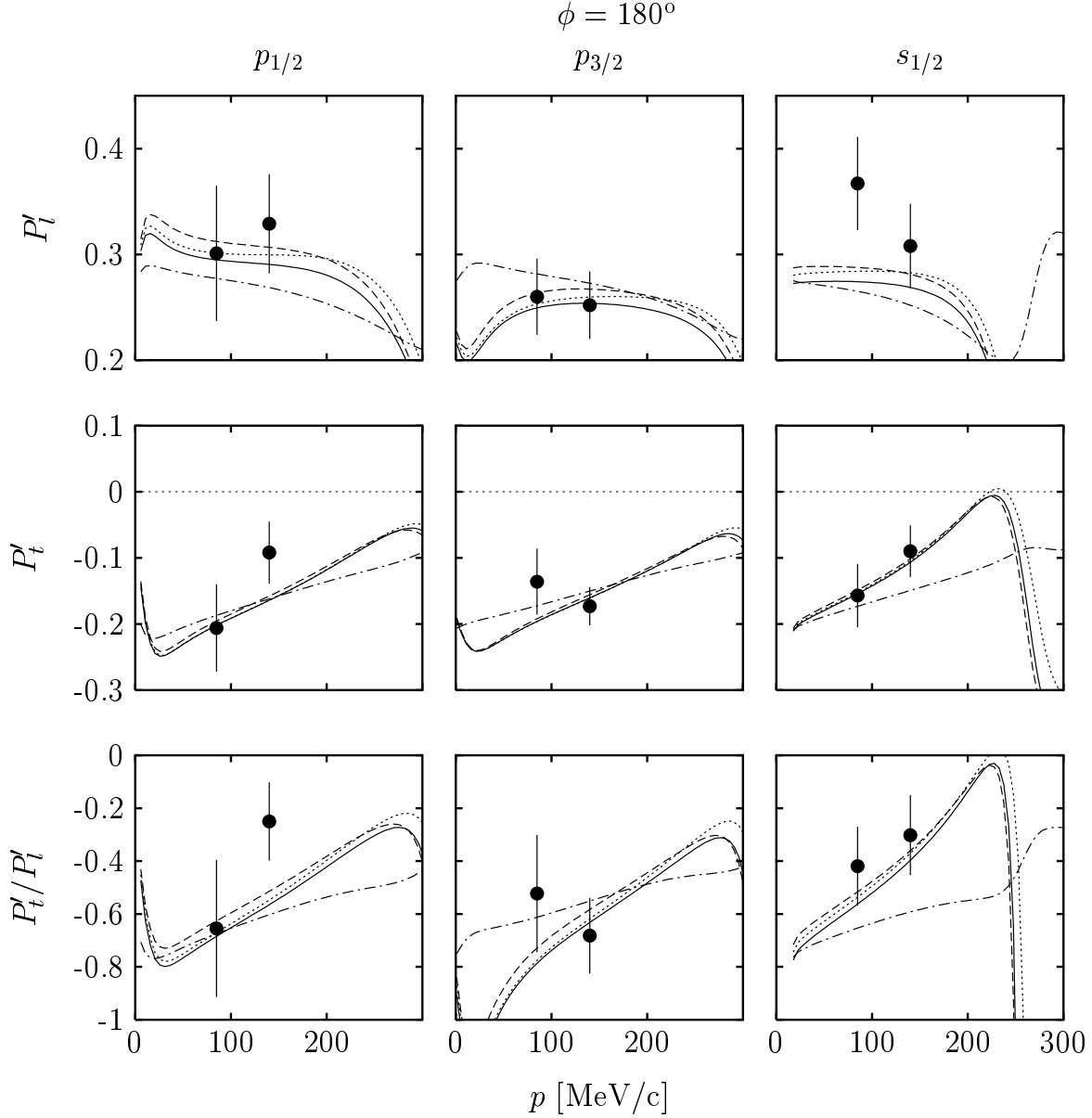


Figure 18: Transferred polarization asymmetries  $P'_l$  and  $P'_t$ , and their quotient  $P'_t/P'_l$  for proton knock-out from the three shells in  $^{16}\text{O}$  for  $q = 1000$  MeV/c and  $\omega = 450$  MeV. The incident electron energy is  $\epsilon_e = 2450$  MeV and the proton azimuthal angle  $\phi = 180^\circ$ . The meaning of the lines is the following: dotted are the DWIA calculation with OB current only; solid are the total OB+MEC result; dot-dashed are also the OB+MEC result but without the spin-orbit term of the optical potential. These three curves have been obtained using the electromagnetic nucleon form factors of Galster. Finally, dashed lines are the total OB+MEC result using instead the form factors of Gari-Krumplemann.

find  $P'_l$  to be the most sensitive one, with a 20% decrease due to the  $\Delta$  for low missing momentum  $p < 200$  MeV/c. In our calculation MEC effects are clearly less important for these missing momentum values.

2. Ryckebusch *et al.* [36] do not present the separate  $l, t, n$  response functions. In general they find small MEC effects, as we do, in the transferred polarizations for low  $p < 300$  MeV/c. These effects being larger as  $q$  and  $p$  increase. Comparing specifically our results to theirs for kinematics II, we observe that the OB results clearly differ due to the different treatment of FSI, while somewhat larger and qualitatively different MEC effects are found in this work.

Be it as it may, since the different treatment of FSI and of the current operators in [33, 36] and in the present work produces discrepancies already at the impulse approximation, it is hard to draw general conclusions on MEC effects beyond the fact that in [33] MEC lead to excessively large contributions compared with us, while their small size in [36] is in accord with our calculation.

## 4 Summary and conclusions

In this paper we have presented a distorted wave model of  $(\vec{e}, e'\vec{p})$  reactions which goes beyond the impulse approximation with the inclusion of two-body meson exchange currents. Relativistic kinematics to relate the energy and momentum of the ejected proton is used and the currents are derived through an expansion in powers of the missing momentum over the nucleon mass. Explicit expressions of the polarized response functions in a general multipole expansion method are given. Results for the responses and transferred polarization asymmetries have been obtained for proton knock-out from the different shells in  $^{16}\text{O}$  for quasiperpendicular kinematics with the transfer momentum fixed to  $q = 460$  and  $1000$  MeV/c. FSI have been considered in each case by using different optical potentials.

One of our primary goals has been to estimate, within our present model, the validity of the impulse approximation by analyzing the effect of MEC on the different recoil nucleon polarized observables. Thus we compare the standard DWIA results, obtained using only the OB current, with the “full” calculation which includes the MEC. We have also explored the role played by the particular description of the FSI, hence we compare the results obtained by using different optical potentials which have been widely considered in the literature: Schwandt [53] and Comfort & Karp [52] parameterizations. For higher energy we have used instead the Schrödinger-equivalent form of a Dirac optical potential.

From our present studies we may summarize and conclude the following:

1. The induced  $T$ ,  $TL$  and  $TT$  polarized responses are particularly sensitive to the details of the optical potential, allowing them, specially the  $TT$  ones, to constrain the theoretical model for FSI. The transferred polarized responses ( $T'$  and  $TL'$ ), which survive in PWIA, show a much less sensitivity to the interaction.

2. In general, MEC effects over the transferred  $T'$ ,  $TL'$  polarized responses for  $q = 460$  MeV/c and moderate missing momentum ( $p < 300$  MeV/c) are rather small ( $< 5\%$ ), and tend to increase as  $q$  goes higher, being of the order of a  $\sim 10\%$  reduction (due mainly to the  $\Delta$  current) in the particular case of  $W_t^{T'}$  and  $q = 1$  GeV/c.

The role of MEC gets clearly more important for the induced  $T$ ,  $TL$  and  $TT$  polarized responses. Emphasis should be placed on  $W_t^{TT}$  and  $W_n^{TT}$  which are reduced at the maximum by  $\sim 20\%$  and  $\sim 30\%$ , respectively, for  $q = 460$  MeV/c and for the  $p_{1/2}$  shell; notice however that these effects are negligible in the case of  $p_{3/2}$ . For  $q = 1$  GeV/c the role of MEC diminishes.

3. FSI give rise to an important deviation of the transferred polarization asymmetries  $P'_t$  and  $P'_l$  with respect to the PWIA results, showing a very pronounced oscillatory behaviour that starts for  $p \geq 200$  MeV/c. This behaviour does not appear in the component  $P'_n$ . The uncertainties introduced by the optical potentials are rather small for the missing momentum region analyzed.
4. MEC effects on  $P'_t$  and  $P'_l$  are negligible for  $q = 460$  MeV/c and increase for  $q = 1$  GeV/c, especially for  $p > 200$  MeV/c. The role of MEC on  $P'_n$  is clearly more important.

Finally we are confident that the significant sensitivity shown by some polarized observables to MEC, particularly to the  $\Delta$  current, will be maintained within the scheme of a “fully” relativistic calculation which takes care of relativistic ingredients, such as the dynamical enhancement of lower components, not included in the present model. Work along this line is in progress.

## Acknowledgments

This work was partially supported by funds provided by DGI (Spain) and FEDER funds, under Contracts Nos BFM2002-03218, BFM2002-03315 and FPA2002-04181-C04-04 and by the Junta de Andalucía.

## A Sum over third components and reduced response functions

In this appendix we perform the sum over third components in the multipole expansion of response functions and give their explicit expressions in terms of the reduced matrix elements of the multipole operators.

First we write the response functions (4–6) in terms of the spherical components of the current matrix elements  $J_{\pm 1} \equiv \langle \mathbf{p}' \mathbf{s}, B | \hat{J}_{\pm 1} | A \rangle$  using the hadronic tensor (7)

$$R^L = \frac{1}{K} \sum \rho^* \rho \quad (67)$$

$$R^T = \frac{1}{K} \sum (|J_{-1}|^2 + |J_{+1}|^2) \quad (68)$$

$$R^{TL} = -2 \frac{1}{K} \text{Re} \sum \rho^* (J_{+1} - J_{-1}) \quad (69)$$

$$R^{TT} = \frac{1}{K} \sum (J_{-1}^* J_{+1} + J_{+1}^* J_{-1}) \quad (70)$$

$$R^{TL'} = -2 \frac{1}{K} \text{Re} \sum \rho^* (J_{+1} + J_{-1}) \quad (71)$$

$$R^{T'} = \frac{1}{K} \sum (|J_{+1}|^2 - |J_{-1}|^2) . \quad (72)$$

$$(73)$$

Inserting the multipole expansion for the charge and current components as given in (23,24) we find that each response can be written as a sum of terms of the type

$$B_{J'J}^{m'm} \equiv \frac{1}{K} \sum_{M_B} \langle \mathbf{p}' \mathbf{s}, J_B M_B | \hat{T}'_{J'm'}(\mathbf{q}) | A \rangle^* \langle \mathbf{p}' \mathbf{s}, J_B M_B | \hat{T}_{Jm}(\mathbf{q}) | A \rangle , \quad (74)$$

where  $\hat{T}'_{J'm'}$  and  $\hat{T}_{Jm}$  represent in general the Coulomb, electric or magnetic multipole operators. Introducing now the multipole expansion (22) corresponding to the final state, which is polarized along an arbitrary direction  $\mathbf{s}$  (8), we get

$$\begin{aligned} B_{J'J}^{m'm} &= \frac{1}{K} \sum_{M_B} \sum_{\nu' \nu} \mathcal{D}_{\nu' \frac{1}{2}}^{(1/2)}(\mathbf{s}) \mathcal{D}_{\nu \frac{1}{2}}^{(1/2)}(\mathbf{s})^* \\ &\times \sum_{l' M' j' m'_p} i^{l'} Y_{l' M'}^*(\hat{\mathbf{p}}') \langle \frac{1}{2} \nu' l' M' | j' m'_p \rangle \langle j' m'_p J_B M_B | J' m' \rangle \langle (l' j') J_B, J' m' | T'_{J'm'} | A \rangle^* \\ &\times \sum_{l M j m_p} i^{-l} Y_{l M}(\hat{\mathbf{p}}') \langle \frac{1}{2} \nu l M | j m_p \rangle \langle j m_p J_B M_B | J m \rangle \langle (l j) J_B, J m | T_{Jm} | A \rangle , \end{aligned} \quad (75)$$

where we have used  $J_f = J$  and  $M_f = m$ , since the initial nucleus has total angular momentum equal zero.

Using the Wigner-Eckart theorem for the matrix elements of tensor operators between states of definite angular momenta

$$\langle (l j) J_B, J m | T_{Jm} | 0 \rangle = \frac{1}{[J]} \langle (l j) J_B, J || T_J || 0 \rangle \quad (76)$$



and reducing the products of two rotation matrices and two spherical harmonics to linear combinations of spherical harmonics

$$\begin{aligned}
\mathcal{D}_{\nu'\frac{1}{2}}^{(1/2)}(\hat{\mathbf{s}})\mathcal{D}_{\nu\frac{1}{2}}^{(1/2)}(\hat{\mathbf{s}})^* &= \sqrt{4\pi} \sum_{\mathcal{J}\mathcal{M}} (-1)^{1/2+\nu+\mathcal{J}} f_{\mathcal{J}}^{(1/2)} \begin{pmatrix} \frac{1}{2} & \frac{1}{2} & \mathcal{J} \\ -\nu & \nu' & \mathcal{M} \end{pmatrix} Y_{\mathcal{J}\mathcal{M}}(\hat{\mathbf{s}}) \quad (77) \\
Y_{\nu'M'}^*(\hat{\mathbf{p}}')Y_{lM}(\hat{\mathbf{p}}') &= \\
&\sum_{\mathcal{J}'\mathcal{M}'} (-1)^M \frac{[l][l'][\mathcal{J}']}{\sqrt{4\pi}} \begin{pmatrix} l & l' & \mathcal{J}' \\ -M & M' & \mathcal{M}' \end{pmatrix} \begin{pmatrix} l & l' & \mathcal{J}' \\ 0 & 0 & 0 \end{pmatrix} Y_{\mathcal{J}'\mathcal{M}'}(\hat{\mathbf{p}}'), \quad (78)
\end{aligned}$$

with  $f_{\mathcal{J}}^{(1/2)} = \frac{1}{\sqrt{2}}$  the Fano tensor for spin-1/2 polarization, we obtain

$$\begin{aligned}
B_{J'J}^{m'm} &= \sum_{M_B} \sum_{\nu\nu'} \sum_{\mathcal{J}\mathcal{M}} \sum_{lM} \sum_{j m_p} \sum_{l' M'} \sum_{j' m'_p} \sum_{\mathcal{J}'\mathcal{M}'} i^{l'-l} (-1)^{\frac{1}{2}+\nu+\mathcal{J}} f_{\mathcal{J}}^{(\frac{1}{2})} \begin{pmatrix} \frac{1}{2} & \frac{1}{2} & \mathcal{J} \\ -\nu & \nu' & \mathcal{M} \end{pmatrix} Y_{\mathcal{J}\mathcal{M}}(\mathbf{s}) \\
&\times (-1)^M [l][l'][\mathcal{J}'] \begin{pmatrix} l & l' & \mathcal{J}' \\ -M & M' & \mathcal{M}' \end{pmatrix} \begin{pmatrix} l & l' & \mathcal{J}' \\ 0 & 0 & 0 \end{pmatrix} Y_{\mathcal{J}'\mathcal{M}'}(\hat{\mathbf{p}}') \\
&\times (-1)^{l'-\frac{1}{2}-m'_p} [j'] \begin{pmatrix} \frac{1}{2} & l' & j' \\ \nu' & M' & -m'_p \end{pmatrix} (-1)^{J_B-j'-m'} \begin{pmatrix} j' & J_B & J' \\ m'_p & M_B & -m' \end{pmatrix} \\
&\times (-1)^{l-\frac{1}{2}-m_p} [j] \begin{pmatrix} \frac{1}{2} & l & j \\ \nu & M & -m_p \end{pmatrix} (-1)^{J_B-j-m} \begin{pmatrix} j & J_B & J \\ m_p & M_B & -m \end{pmatrix} \\
&\times \langle (l'j')J_B, J' \| T_{J'} \| 0 \rangle^* \langle (lj)J_B, J \| T_J \| 0 \rangle, \quad (79)
\end{aligned}$$

where we have transformed the Clebsch-Jordan to three-J coefficients. Next we perform the sums over third components of angular momenta in the above expression. Note that the total phase inside the sum can be simplified to

$$\text{phase} = (-1)^{\frac{1}{2}+m_p} (-1)^{\mathcal{J}+l+l'} (-1)^{j-j'}. \quad (80)$$

Therefore the following coefficient appears

$$\begin{aligned}
S &\equiv \sum_{M_B} \sum_{\nu\nu'} \sum_{MM'} \sum_{m_p m'_p} (-1)^{\frac{1}{2}+m_p+\mathcal{J}+l+l'+j-j'} \begin{pmatrix} \frac{1}{2} & \frac{1}{2} & \mathcal{J} \\ -\nu & \nu' & \mathcal{M} \end{pmatrix} \begin{pmatrix} l & l' & \mathcal{J}' \\ -M & M' & \mathcal{M}' \end{pmatrix} \\
&\times \begin{pmatrix} \frac{1}{2} & l' & j' \\ \nu' & M' & -m'_p \end{pmatrix} \begin{pmatrix} j' & J_B & J' \\ m'_p & M_B & -m' \end{pmatrix} \begin{pmatrix} \frac{1}{2} & l & j \\ \nu & M & -m_p \end{pmatrix} \begin{pmatrix} j & J_B & J \\ m_p & M_B & -m \end{pmatrix}. \quad (81)
\end{aligned}$$

We first perform the sum over  $\nu, \nu', M, M'$  by using a 9-j coefficient

$$\begin{aligned} & \sum_{\nu\nu'} \sum_{MM'} \begin{pmatrix} \frac{1}{2} & \frac{1}{2} & \mathcal{J} \\ -\nu & \nu' & \mathcal{M} \end{pmatrix} \begin{pmatrix} l & l' & \mathcal{J}' \\ -M & M' & \mathcal{M}' \end{pmatrix} \begin{pmatrix} \frac{1}{2} & l & j \\ \nu & M & -m_p \end{pmatrix} \begin{pmatrix} \frac{1}{2} & l' & j' \\ \nu' & M' & -m'_p \end{pmatrix} = \\ & (-1)^{\frac{1}{2}+l+j} \sum_{LM} [L]^2 \begin{pmatrix} \mathcal{J} & \mathcal{J}' & L \\ \mathcal{M} & \mathcal{M}' & M \end{pmatrix} \begin{pmatrix} L & j & j' \\ M & m_p & -m'_p \end{pmatrix} \left\{ \begin{matrix} \mathcal{J} & \mathcal{J}' & L \\ \frac{1}{2} & l & j \\ \frac{1}{2} & l' & j' \end{matrix} \right\}. \end{aligned} \quad (82)$$

Next we compute the sum over  $m_p, m'_p, M_B$  using a 6-j coefficient

$$\begin{aligned} & \sum_{m_p m'_p M_B} (-1)^{m_p + \frac{1}{2}} \begin{pmatrix} L & j & j' \\ M & m_p & -m'_p \end{pmatrix} \begin{pmatrix} j & J_B & J \\ m_p & M_B & -m \end{pmatrix} \begin{pmatrix} j' & J_B & J' \\ m'_p & M_B & -m' \end{pmatrix} = \\ & (-1)^{\frac{1}{2}+m'+j+j'+J_B} \begin{pmatrix} L & J' & J \\ M & -m' & m \end{pmatrix} \left\{ \begin{matrix} L & J' & J \\ J_B & j & j' \end{matrix} \right\}. \end{aligned} \quad (83)$$

Then the  $S$ -coefficient (81) results

$$\begin{aligned} S &= \sum_{LM} [L]^2 (-1)^{\mathcal{J}+l'+j+J_B+m'} \begin{pmatrix} L & J' & J \\ M & -m' & m \end{pmatrix} \begin{pmatrix} \mathcal{J} & \mathcal{J}' & L \\ \mathcal{M} & \mathcal{M}' & M \end{pmatrix} \\ & \times \left\{ \begin{matrix} \mathcal{J} & \mathcal{J}' & L \\ \frac{1}{2} & l & j \\ \frac{1}{2} & l' & j' \end{matrix} \right\} \left\{ \begin{matrix} L & J' & J \\ J_B & j & j' \end{matrix} \right\}. \end{aligned} \quad (84)$$

To finish we insert the result (84) into (79), and define indices  $\sigma, \sigma'$  corresponding to the quantum numbers of the final states

$$\sigma = (l, j, J), \quad \sigma' = (l', j', J') \quad (85)$$

and a coupling coefficient

$$\begin{aligned} \Phi_{\sigma'\sigma}(\mathcal{J}, \mathcal{J}', L) &= \sqrt{2} [l] [l'] [j] [j'] [J] [J'] [\mathcal{J}] [L] (-1)^{l+j+J_B+L+J+J'} \\ & \times \begin{pmatrix} l & l' & \mathcal{J}' \\ 0 & 0 & 0 \end{pmatrix} \left\{ \begin{matrix} L & J' & J \\ J_B & j & j' \end{matrix} \right\} \left\{ \begin{matrix} \mathcal{J} & \mathcal{J}' & L \\ \frac{1}{2} & l & j \\ \frac{1}{2} & l' & j' \end{matrix} \right\}. \end{aligned} \quad (86)$$

The final expression for  $B$  is

$$\begin{aligned} B_{J'J}^{m'm} &= \frac{1}{2} \sum_{lj} \sum_{l'j'} \sum_{\mathcal{J}\mathcal{J}'LM} i^{l'-l} (-1)^m \begin{pmatrix} J & J' & L \\ m & -m' & M \end{pmatrix} \Phi_{\sigma'\sigma}(\mathcal{J}, \mathcal{J}', L) \\ & \times [Y_{\mathcal{J}}(\hat{\mathbf{s}}) Y_{\mathcal{J}'}(\hat{\mathbf{p}}')]_{L, -M} \langle (l'j') J_B, J' \| T_{J'} \| 0 \rangle^* \langle (lj) J_B, J \| T_J \| 0 \rangle, \end{aligned} \quad (87)$$

where the coupling between two spherical harmonics has been used

$$\begin{aligned}
& [Y_{\mathcal{J}}(\hat{\mathbf{s}})Y_{\mathcal{J}'}(\hat{\mathbf{p}}')]_{LM} = \\
& = (-1)^{\mathcal{J}-\mathcal{J}'+M} \sum_{\mathcal{M}\mathcal{M}'} [L] \begin{pmatrix} \mathcal{J} & \mathcal{J}' & L \\ \mathcal{M} & \mathcal{M}' & -M \end{pmatrix} Y_{\mathcal{J}\mathcal{M}}(\hat{\mathbf{s}})Y_{\mathcal{J}'\mathcal{M}'}(\hat{\mathbf{p}}').
\end{aligned} \tag{88}$$

Although the result given in eq. (87) is formally identical, with the exception of the factor  $1/2$ , to the one obtained in [49] for the case of polarized nuclei, there exists a basic difference concerning the polarization coefficient  $\Phi_{\sigma'\sigma}(\mathcal{J}, \mathcal{J}', L)$ , which contains all the information on the polarization properties of the particles in the initial and/or final state. Note that in the present case (spin-1/2 polarized particles), the angular momentum in the expansion of the rotation matrices,  $\mathcal{J}$ , only takes the values 0,1. The case  $\mathcal{J} = 0$  is the only one surviving when the final nucleon is not polarized, i.e., when summing the cross sections for  $\pm s$  values. In this case the present formalism reduces simply to the standard unpolarized one of ref. [41]. In fact, for  $\mathcal{J} = 0$  we have  $\mathcal{J}' = L$  and the reader can prove after some Racah algebra, that  $\Phi_{\sigma'\sigma}(0, L, L)$  reduces to the expression given in eq. (A11) of Ref. [41] for the unpolarized case.

Moreover, using the properties of the 9-j symbol, the following important symmetry property is found for the polarization coefficient under exchange of the indices

$$\Phi_{\sigma'\sigma}(\mathcal{J}, \mathcal{J}', L) = (-1)^{\mathcal{J}+\mathcal{J}'+L} \Phi_{\sigma\sigma'}(\mathcal{J}, \mathcal{J}', L). \tag{89}$$

This property coincides with the one already presented in [49] in the case of polarized targets. Since the multipole expansion of response functions performed in [49] was based on this symmetry, then the same formalism can be applied to the present case. In this way one arrives to eqs. (37–45) (see [49] for more details on the expansion).

## References

- [1] S. Frullani and J. Mougey, *Adv. Nucl. Phys.* **14** (1984) 1
- [2] S. Boffi, C. Giusti, F.D. Pacati, *Phys. Rep.* 226 (1993) 1.
- [3] J. J. Kelly, *Adv. Nucl. Phys.* **23** (1996) 75.
- [4] S. Boffi, C. Giusti, F. D. Pacati, M. Radici, *Electromagnetic response of atomic nuclei*, Oxford University Press (1996).
- [5] Y. Jin, D.S. Onley, L.E. Wright, *Phys. Rev. C* **50** (1994) 168.
- [6] M. K. Gaidarov, K. A. Pavlova, A. N. Antonov, M. V. Stoitsov, S. S. Dimitrova, M.V. Ivanov and C. Giusti, *Phys. Rev. C* **61** (2000) 014306.

- [7] J.M. Udías, P. Sarriguren, E. Moya de Guerra, E. Garrido, J.A. Caballero, Phys. Rev. C **48**(1993) 2731; **51** (1995) 3246.
- [8] J.M. Udias, J.A. Caballero, E. Moya de Guerra, J. R. Vignote, A. Escuderos, Phys.Rev. C64 (2001) 024614.
- [9] J.J. Kelly and S.J. Wallace, Phys. Rev. C **49**, 1315 (1994).
- [10] J.E. Amaro, G. Co', A.M. Lallena, Ann. Phys. (N.Y.) **221**, 306 (1993).
- [11] J.E. Amaro, G. Co', A.M. Lallena, Nucl. Phys. **A** 578, 365 (1994).
- [12] D.O. Riska, Phys. Rep. **181** (1989) 208; J.F. Mathiot, Phys. Rep. **173** (1989) 64.
- [13] J. M. Udias, J. A. Caballero, E. Moya de Guerra, J. E. Amaro and T. W. Donnelly, Phys. Rev. Lett. 83 (1999) 5451.
- [14] L. Chinitz *et al.*, Phys. Rev. Lett. **67** (1991) 568.
- [15] C.M. Spaltro *et al.*, Phys. Rev. **C48** (1993) 2385
- [16] J. Gao *et al.*, Phys. Rev. Lett. 84 (2000) 3265.
- [17] J.J. Kelly, Phys. Rev. C **60** 044609 (1999).
- [18] D. Debruyne, J. Ryckebusch, W. Van Nespén, and S. Janssen, Phys. Rev. C **62** 024611 (2000).
- [19] J.A. Caballero, M.C. Martinez, E. Moya de Guerra, J.M. Udias, J.E. Amaro, and T.W. Donnelly, Nucl. Phys. A **689** 449c (2001).
- [20] J. Mandeville *et al.*, Phys. Rev. Lett. **72**, 3325 (1994).
- [21] R.J. Woo *et al.*, Phys. Rev. Lett. **80**, 456 (1998).
- [22] S. Malov *et al.*, Phys. Rev. C **62**, 057302 (2000).
- [23] A. Picklesimer, J.W. Van Orden, Phys. Rev. C **35** 266 (1987).
- [24] A. Picklesimer and J.W. Van Orden, Phys. Rev. C **40**, 290 (1989).
- [25] J.I. Johansson and H.S. Sherif, Phys. Rev. C **59** 3481 (1999).
- [26] J.M. Udias, J.R. Vignote, Phys. Rev. C **62** 034302 (2000).
- [27] J.J. Kelly, Phys. Rev. C **59** 3256 (1999).
- [28] H. Ito, S.E. Koonin, R. Seki, Phys. Rev. C **56** 3231 (1997).
- [29] D. Debruyne, J. Ryckebusch, S. Janssen, and T. Van Cauteren, Phys. Lett. B **527** 62 (2002).

- [30] M.C. Martinez, J.A. Caballero, T.W. Donnelly, Nucl. Phys. A **707** 83 (2002).
- [31] M.C. Martinez, J.A. Caballero, T.W. Donnelly, Nucl. Phys. A **707** 121 (2002).
- [32] M.C. Martínez, *et al.*, In preparation (2003).
- [33] S. Boffi, C. Giusti, F.D. Pacati and M. Radici, Nucl. Phys. A **518** 639 (1990).
- [34] S. Boffi, M. Radici, Nucl. Phys. A **526** 602 (1991).
- [35] J. Ryckebusch, Phys. Rev. C **64** 044606 (2001).
- [36] J. Ryckebusch, D. Debruyne, W. Van Nespén, and S. Janssen, Phys. Rev. C **60** 034604 (1999).
- [37] V. Van der Sluys, J. Ryckebusch, and M. Waroquier, Phys. Rev. C **49** 2695 (1994).
- [38] J.E. Amaro, A.M. Lallena, and J.A. Caballero, Phys. Rev. C **60** 014602 (1999).
- [39] C. Giusti, F.D. Pacati, Phys. Rev. C **67** 044601 (2003)
- [40] J.E. Amaro, M.B. Barbaro, J.A. Caballero, and F. Kazemi Tabatabaei, Phys. Rev. C in press, nucl-th/0302004,
- [41] M. Mazziotta, J.E. Amaro, F. Arias de Saavedra, Phys. Rev. C **65** (2002) 034602.
- [42] J.E. Amaro, J.A. Caballero, T.W. Donnelly, E. Moya de Guerra, A.M. Lallena, and J.M. Udias, Nucl. Phys. A **602** (1996) 263.
- [43] J.E. Amaro, J.A. Caballero, T.W. Donnelly, and E. Moya de Guerra Nucl. Phys. A **611** (1996) 163.
- [44] J.E. Amaro, M.B. Barbaro, J.A. Caballero, T.W. Donnelly, A. Molinari, Nucl. Phys. **A643** (1998) 349.
- [45] J.E. Amaro, M.B. Barbaro, J.A. Caballero, T.W. Donnelly, A. Molinari, Phys. Rep. **368** (2002) 317.
- [46] J.E. Amaro, M.B. Barbaro, J.A. Caballero, T.W. Donnelly, A. Molinari, Nucl. Phys. A **723** (2003) 181.
- [47] A. Meucci, C. Giusti, F.D. Pacati, Phys. Rev. C **66** 034610 (2002).
- [48] A.S. Raskin and T.W. Donnelly, Ann. Phys. (N.Y.) **191** 78 (1989).
- [49] J.E. Amaro and T.W. Donnelly, Ann. Phys. (N.Y.) **263** 56 (1998).
- [50] S. Galster et al., Nucl. Phys. **B32**, 221 (1971).
- [51] F. Kazemi Tabatabaei, J.E. Amaro, J.A. Caballero, In preparation.

- [52] J.R. Comfort and B.C. Karp, Phys. Rev. C **21**, 2162 (1980).
- [53] P. Schwandt *et. al.*, Phys. Rev. C **26** 55 (1982).
- [54] E.D. Cooper, S. Hama, B.C. Clark, R.L. Mercer, Phys. Rev. C **47**, 297 (1993).
- [55] R.G. Arnold, C.E. Carlson, F. Gross, Phys. Rev. C **23** (1981) 363.
- [56] M. Gari, W. Krumplemann, Z. PHYS. A **322**, 689 (1985)
- [57] J.M. Udias (private communication).